AD_____

Award Number: W81XWH-10-1-0562

TITLE: Improved Image-Guided Laparoscopic Prostatectomy

PRINCIPAL INVESTIGATOR: Ioana Fleming

CONTRACTING ORGANIZATION: The Johns Hopkins University
Baltimore, MD 21218

REPORT DATE: August 2012

TYPE OF REPORT: Annual Summary

PREPARED FOR: U.S. Army Medical Research and Materiel Command
Fort Detrick, Maryland 21702-5012

DISTRIBUTION STATEMENT: Approved for public release; distribution unlimited

The views, opinions and/or findings contained in this report are those of the author(s) and should not be construed as an official Department of the Army position, policy or decision unless so designated by other documentation.

REPORT DOCUMENTATION PAGE

Form Approved
OMB No. 0704-0188

Public reporting burden for this collection of information is estimated to average 1 hour per response, including the time for reviewing instructions, searching existing data sources, gathering and maintaining the data needed, and completing and reviewing this collection of information. Send comments regarding this burden estimate or any other aspect of this collection of information, including suggestions for reducing this burden to Department of Defense, Washington Headquarters Services, Directorate for Information Operations and Reports (0704-0188), 1215 Jefferson Davis Highway, Suite 1204, Arlington, VA 22202-4302. Respondents should be aware that notwithstanding any other provision of law, no person shall be subject to any penalty for failing to comply with a collection of information if it does not display a currently valid OMB control number. **PLEASE DO NOT RETURN YOUR FORM TO THE ABOVE ADDRESS.**

1. REPORT DATE *(DD-MM-YYYY)*	2. REPORT TYPE	3. DATES COVERED *(From - To)*
01-08-2012	Annual Summary	15 JUL 2011 - 14 JUL 2012

4. TITLE AND SUBTITLE
Improved Image-Guided Laparoscopic Prostatectomy

5a. CONTRACT NUMBER

5b. GRANT NUMBER
W81XWH-10-1-0562

5c. PROGRAM ELEMENT NUMBER

6. AUTHOR(S)
Ioana Fleming

E-Mail: inicola1@jhu.edu

5d. PROJECT NUMBER

5e. TASK NUMBER

5f. WORK UNIT NUMBER

7. PERFORMING ORGANIZATION NAME(S) AND ADDRESS(ES)
The Johns Hopkins University
Baltimore, MD 21218

8. PERFORMING ORGANIZATION REPORT NUMBER

9. SPONSORING / MONITORING AGENCY NAME(S) AND ADDRESS(ES)
U.S. Army Medical Research and Materiel Command
Fort Detrick, Maryland 21702-5012

10. SPONSOR/MONITOR'S ACRONYM(S)

11. SPONSOR/MONITOR'S REPORT NUMBER(S)

12. DISTRIBUTION / AVAILABILITY STATEMENT
Approved for Public Release; Distribution Unlimited

13. SUPPLEMENTARY NOTES

14. ABSTRACT

Ex-vivo prostate specimens study was completed using standard ultrasound probe as an equivalent to the LAPUS probe. Data was analyzed and the results show elastography has the potential to detect prostate cancer through direct interrogation techniques. Scientific findings were published in the Medical Science Monitor Journal. A phantom study using a modified prostate elastography phantom was completed. LAPUS and TRUS probe were compared and the results show feasibility in lesion detection with elastography but there are concerns about probe manipulation due to its size. An animal study to better evaluate usability and performance of LAPUS probe is planned for the next 9 months. Clinical, prostate cancer and engineering education and training are on track.

15. SUBJECT TERMS
Prostate Cancer, Ultrasound Elastography

16. SECURITY CLASSIFICATION OF:			17. LIMITATION OF ABSTRACT	18. NUMBER OF PAGES	19a. NAME OF RESPONSIBLE PERSON
a. REPORT	b. ABSTRACT	c. THIS PAGE			USAMRMC
U	U	U	UU	40	19b. TELEPHONE NUMBER *(include area code)*

Table of Contents

Page

1. INTRODUCTION

Prostate cancer is the second leading cause of cancer death and the most common cancer detected in men in the United States. Radical Prostatectomy (RP) is a surgical procedure with a goal of complete cancer resection. Open radical prostatectomies are associated with loss of blood and lengthy recovery times. Laparoscopic radical prostatectomies (LRP) have a very steep learning curve, lack 3-D visualization and use rigid, stick-like instruments which hinder the dissection. A third technique has recently emerged; laparoscopy using the daVinci Surgical System (Intuitive Surgical, Sunnyvale, CA). The surgical robot introduces many benefits, including three-dimensional visualization, higher magnification, hand tremor elimination and refined dexterity by incorporating wristed instrumentation. Robotic-assisted laparoscopic prostatectomy (RALP) strives to maximize tumor resection and nerve preservation and it has rapidly become the preferred surgical approach. Recent studies have showed RALP is a feasible procedure with a short learning curve, limited blood loss, less post-ostoperative pain, favorable complication rates, and short hospital stay. The lack of tactile feedback is however, one theoretical disadvantage that has been raised with regards to robotic surgery. There is a need for real-time intraoperative guidance in laparoscopic prostatectomies. Hence the objective of this proposal is to develop such a capability. Ultrasound Elastography (USE) is a technology which can be integrated with the robotic probe. Elastography is ideal as a technology as it allows for real-time acquisition of images of the prostate gland and, similar to human palpation, allows for contact based interrogation of the prostate's surface [1]. USE is affordable and minimally invasive and can also be miniaturized and incorporated into robotically assisted prostatectomy. USE using a laparoscopic ultrasound probe (LAPUS) can help the surgeon visualize the anatomy of the prostate gland, identify the contours of the cancerous tumors as well as any extra capsular extension. The contribution of the proposed research project is that it will allow for real-time intraoperative acquisition of images of the prostate gland and the surrounding tissues. We are proposing a safe, simple and robust technique for direct interrogation of the prostate surface aided by a laparoscopic US probe. USE will be a valuable tool in the identification of cancerous lesions and the trajectory of cavernous nerves and thus improve the chances for a cancer-free, nerve-sparing outcome.

2. BODY

This report will address each of the tasks we proposed to accomplish in the Statement of Work as outlined in Table 1.

	Year 1	Year 2	Year 3 (9 months)
Task 2. System Integration and Clinical Evaluation			
2a. Integration, testing, pre-operative plan			
2b. IRB approval			
2c. Clinical study (N= 5-10)			
Task 3. Design and build new LAPUS probe			
3a. Evaluate data from clinical study			
3b. Design and build New LAPUS probe			
3c. Automatic robotic-assisted palpation			
Task 4. Laparoscopic Prostatectomy with Advanced US Imaging Methods			
4a. Probe evaluation - phantoms			
4b. Probe evaluation – animal models			
4c. Cavernous nerves imaging			

Table 1: Statement of Work for Engineering Tasks 2,3,4

Last year in the first annual report we were reporting among our accomplishments the completion of tasks **2a**, **3c**, and an improvement in our ultrasound elastography method which contributed towards accomplishing

tasks **4a-c**. The scientific papers supporting these accomplishments have been published in their final form in February 2012 and are attached as Appendix 1, 2 and 3 respectively:

1. Fleming, I., Rivaz, H., Boctor, E., Hager, G. "*Robust Dynamic Programming Method for Ultrasound Elastography*", Proceedings of SPIE Medical Imaging, San Diego, CA, February 2012 - published paper
2. Fleming, I., Rivaz, H., Boctor, E., Hager, G. "*Robust Dynamic Programming Method for Ultrasound Elastography*", Proceedings of SPIE Medical Imaging, San Diego, CA, February 2012 - presented poster.
3. Billings, S., Nishikant, D., Kang, H. J., Taylor, R., Boctor, E., "*System for robot-assisted real-time laparoscopic ultrasound elastography*," Proceedings of SPIE Medical Imaging, San Diego, CA, February 2012 - published paper

At the end of the first year, we had not yet achieved tasks **2b IRB approval (months 1-6) and 2c. Clinical evaluation (months 6-12)**. Having been experiencing delays in the submission of the IRB proposal, out team debated how to best accomplished the proposed project goals in the time left available. Our goals were to evaluate the capabilities of the Laparoscopic Ultrasound (LAPUS) probe (Figure 1) in imaging prostate cancerous tissue and also to prepare for clinical testing of LAPUS as an imaging tool during robotic-assisted laparoscopic prostatectomy.

Figure 1: LAPUS Probe

Existing ultrasound data from *ex-vivo* prostate specimens (collected recently by our team as part of an IRB approved, ongoing study) were used to asses the capability of a standard ultrasound probe Siemens VF10-5 linear array with similar capabilities/transducer with the LAPUS probe. **N = 6** prostate specimens from patients enrolled in our study, provided **N = 10** target areas, **8** hard nodules in the peripheral zone, **1** hard and **1** soft nodule in the central part of the gland. Data from this clinical study was evaluated (**Task 3a**) and the elastography findings compared favorably with pathology reports and MRI findings - Figure 2 and Table 2.

Our analysis proves that an ultrasound probe fitted with a transducer similar with our LAPUS probe, can produce elastograms which can help the surgeon identify hard and soft lesions in the prostate tissue. We submitted our findings and our paper has been accepted for publication in the Medical Science Monitor Journal. The final proof of the paper which will be published in the upcoming issue of the journal is attached to this report as Appendix 4:

Ioana Nicolaescu Fleming, Carmen Kut, Katarzina Macura, Li-Ming Su, Hassan Rivaz, Caitlin Schneider, Ulrike Hamper, Tamara Lotan, Russ Taylor, Gregory Hager, Emad Boctor, " *Ultrasound elastography as a tool for imaging guidance during prostatectomy: Initial experience*", Med Sci Monit, 2012; 18(9)

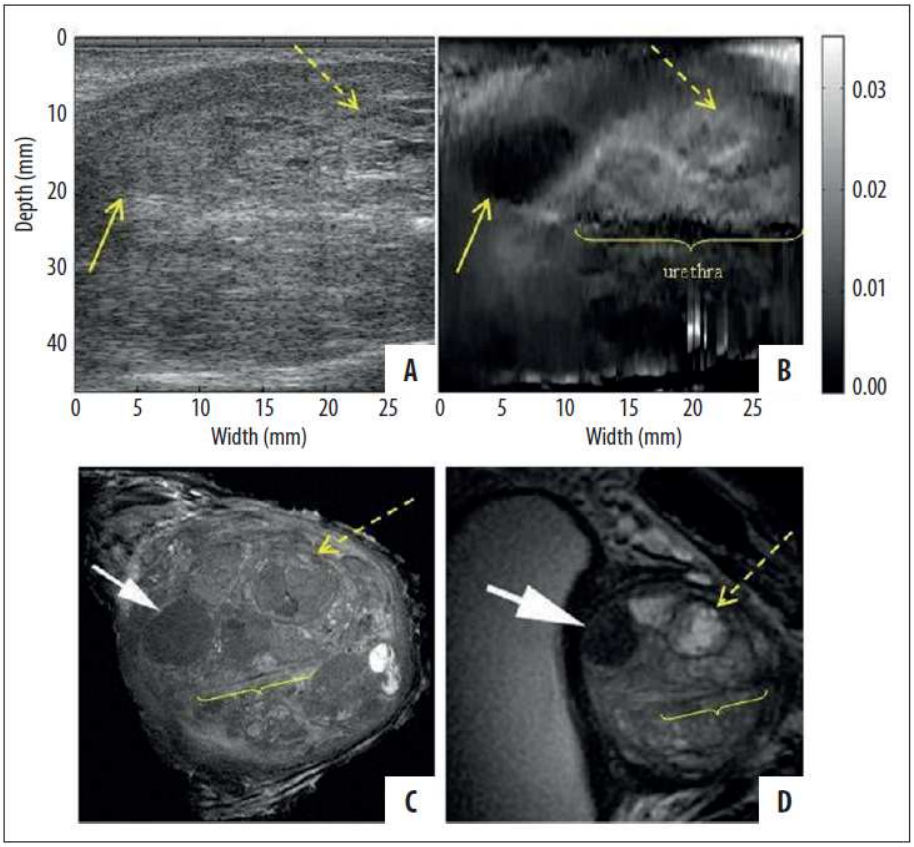

Figure 2: Coronal section of prostate specimen #1 at the level of the central gland. Classic ultrasound B-mode (A) and elastogram (B). 9.4 Tesla *ex-vivo* (C) and 3 Tesla *in-vivo* (D) MRI images are presented in coronal planes, in CCW (counter clock wise) orientation for better visualization of the correlation between USE and MRI of the specimen. Benign solid (arrow) and soft(dashed arrow) nodules and urethra are visible.

Table 2. Prostate specimen data: A total of 10 (ten) elastography lesions were identified in 6 (six) patients' specimens (8 malignant and 2 benign).

#	Location	Gleason score	Size (cm)		
			Elastography	Pathology	MRI
1.1	PZ base	3+5	1.4×0.8	1.3×0.8	1.3×1.1
1.2	CG base	N/A-Solid	0.7×1.1	1.0×1.0	1.0×1.1
1.3	CG base	N/A-Soft	1.1×0.8	1.0×1.0	1.0×0.9
2.1	PZ base	5+3	3.0×1.3	2.4×1.0	2.0×1.5
3.1	PZ mid	4+5	2.4×0.8	1.9×1.0	1.5×1.2
4.1	PZ mid	3+3	1.0×0.5	0.5×0.4	0.6×0.7
4.2	PZ mid	3+4	1.5×0.9	1.1×0.5	1.1×0.8
5.1	PZ apex	3+3	0.5×0.6	0.5×0.5	0.6×0.6
5.2	PZ apex	4+3	0.6×1.0	0.8×0.9	0.9×0.9
6.1	PZ base	3+3	0.7×1.2	0.7×1.8	0.7×0.7

PZ – peripheral zone; CG – central gland.

Having used a standard ultrasound probe as a surrogate for the LAPUS probe's capabilities, we still had to evaluate the ability of the probe to access and interrogate the surface of the prostate in a robotic-assisted approach. For our goal we employed a custom made prostate elastography phantom (CIRS, Inc. - Model 066). The phantom was modified and it's top was removed to allow for LAPUS probe access and imaging through direct contact - Figure 3.

Figure 3: Modified CIRS 066 Prostate Elastography phantom. The top has been removed and direct access to the prostate-mimicking tissue was made available.

The Model 066 contains 3 isoechoic lesions that are at least two times stiffer than the simulated prostate tissue. Under normal ultrasound they cannot be detected but are readily visible on elastograms - Figure 4.

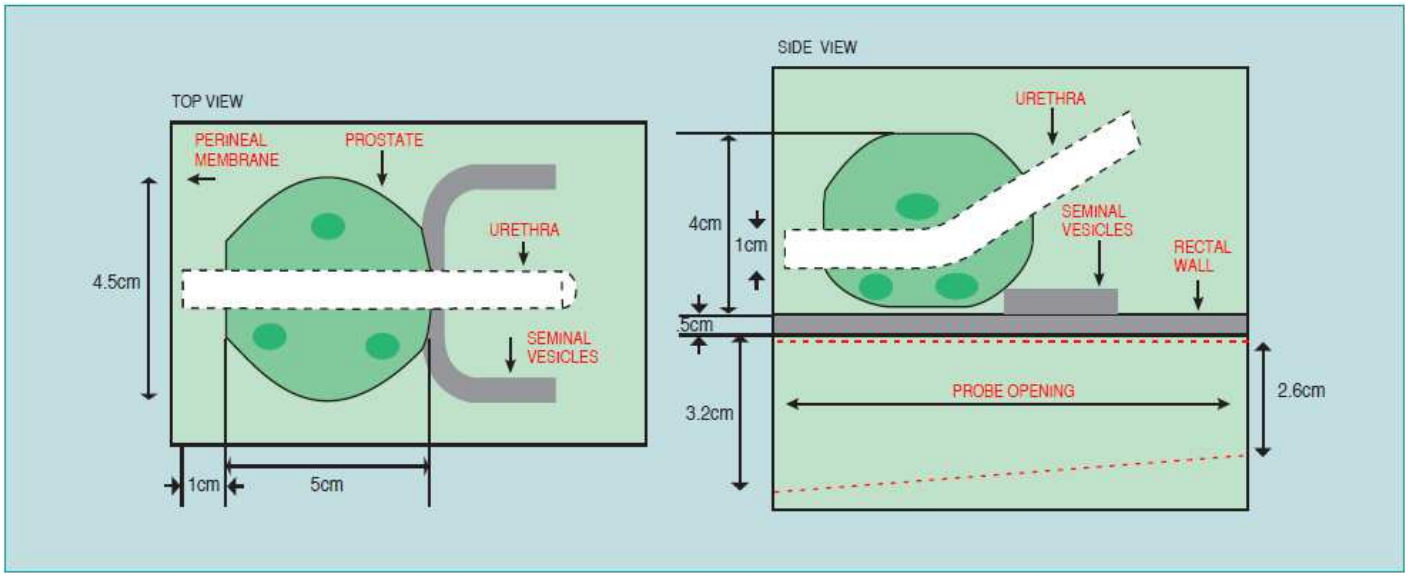

Figure 4: Position of stiffer lesions inside the Model 066 phantom.

We attempted to image the lesions inside the phantom using the LAPUS probe is comparison with a transrectal ultrasound (TRUS) probe - Figure 5. The phantom allows for rectal-like examination and the TRUS probe is routinely used in practice for imaging the prostate tissue during biopsies and sometimes during prostatectomies.

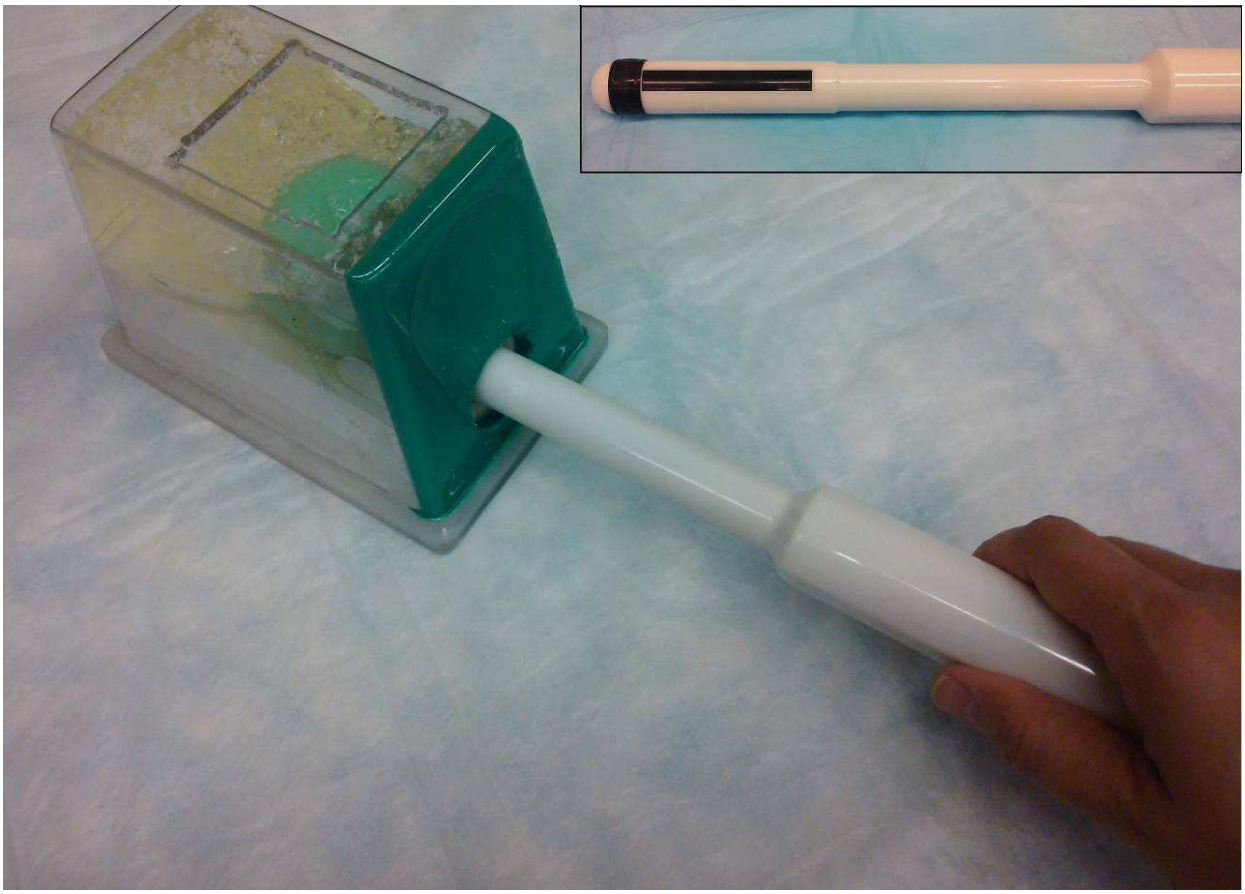

Figure 5: TRUS probe in use with the prostate elastography phantom.

The LAPUS probe presented some challenges we took note of, particularly its length appeared big with respect to the size of the prostate. If a custom probe is to be built in the future just for prostatectomy, it is our conclusion that is should be shorter then the current size of our LAPUS probe. Even though the size presented a challenge, we were able to image a majority of the prostate mimicking tissue. Palpation with the probe was needed in order to identify the stiffer lesions using our elastography algorithm - Figure 6.

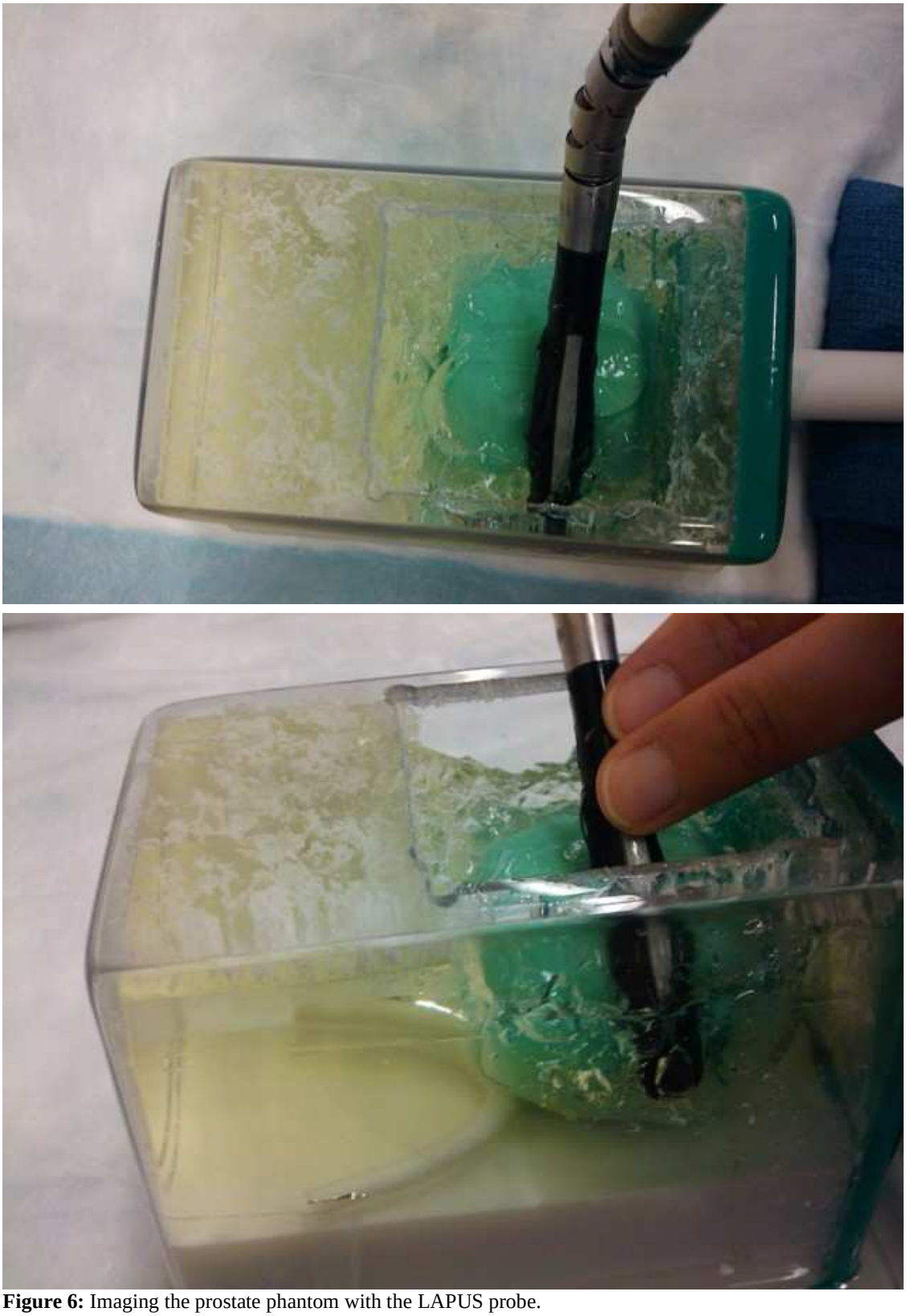

Figure 6: Imaging the prostate phantom with the LAPUS probe.

Our analysis showed that LAPUS was just as capable as TRUS probe in identifying the stiffer lesions. One important thing to mention is that in order to obtain elastograms with TRUS, we applied compression on the tissue from the top, which is equivalent to palpating the prostate during prostatectomy. Classic B-mode ultrasound and elastograms obtained using TRUS are presented in Figure 7, and the corresponding findings using LAPUS are shown in Figure 8. Our findings are being drafted for publication for the Proceedings of SPIE Medical Imaging to take place in Orlando, FL in February 2013.

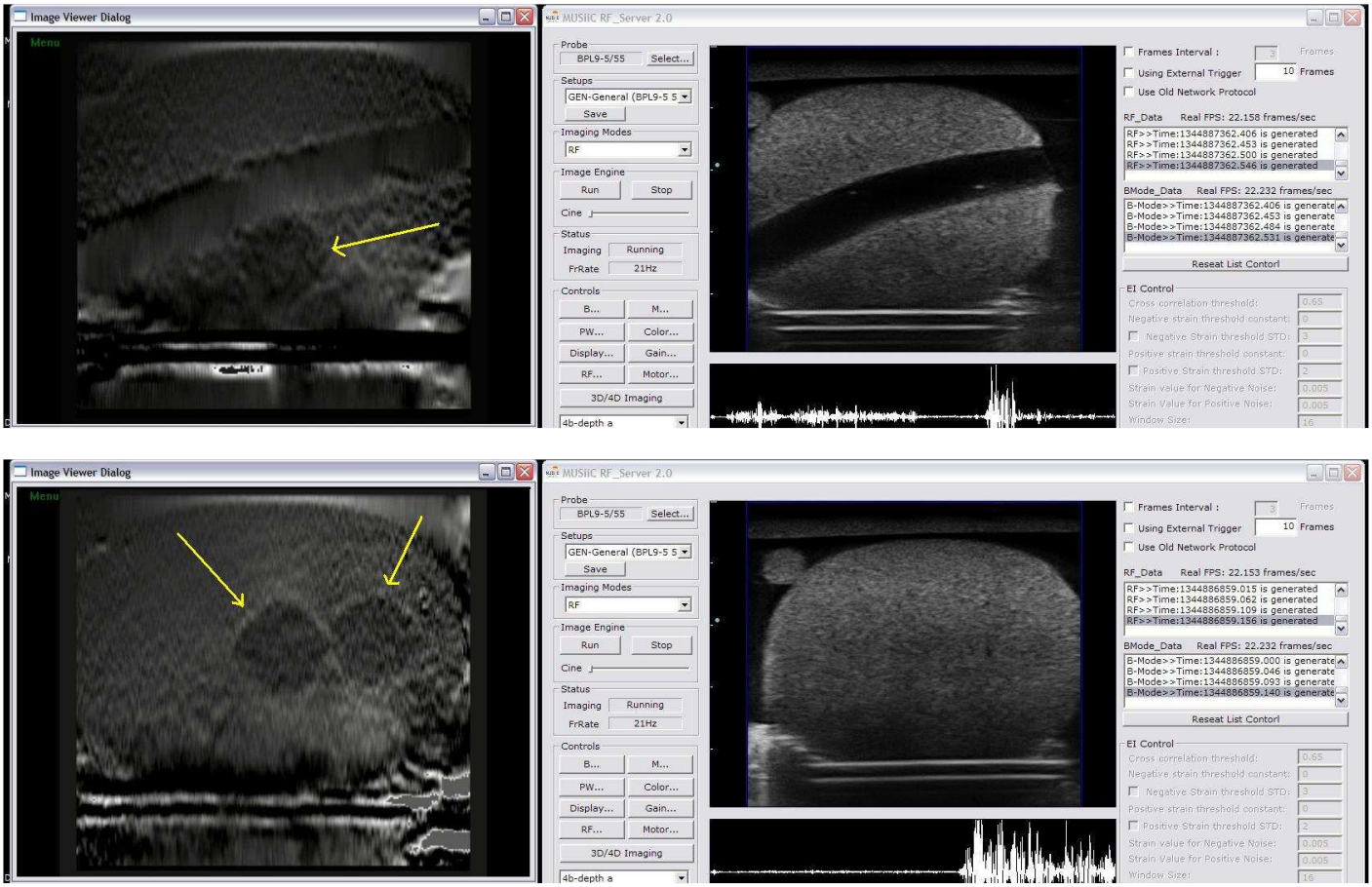

Figure 7: Elastogram and classic B-mode ultrasound for 3 stiff lesions inside prostate phantom Model 066 - TRUS probe imaging

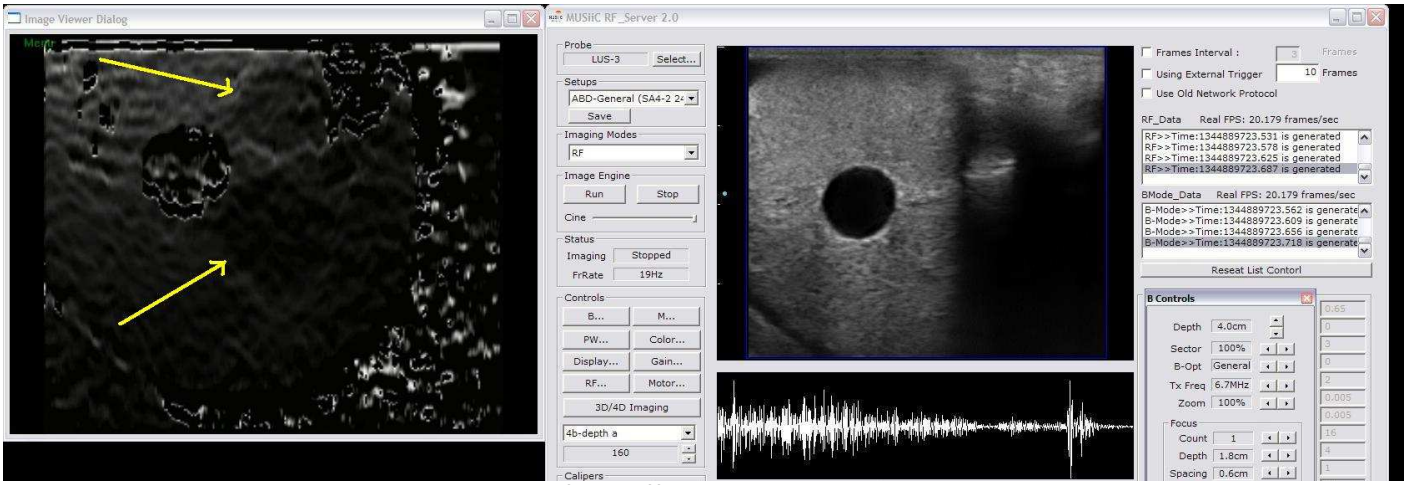

Figure 8: Elastogram and classic B-mode ultrasound for 3 stiff lesions inside prostate phantom Model 066 - LAPUS probe imaging

With this study we consider accomplished **Task 4a.** For the remaining 9 months of our fellowship we are in the process of planning an animal study (**Task** 4b) for the evaluation of the surgical technique, ease of use and potential hurdles in the adoption of the LAPUS probe in robot-assisted laparoscopic prostatectomy. We are currently drafting a protocol for the IRB approval of the proposed animal study. I am actively working with (and learning from) our urology surgeons and

residents to put together a series of tasks for the study. We intend to compare the performance and ease of use of our robotic LAPUS probe with a standard rigid laparoscopic ultrasound probe and with the transrectal TRUS probe.

Advances have also been made in improving the robustness of our elastography algorithm. We have added the capability for 2D and 3D mosaics. Our work was submitted for publication - Appendix 5:

Fleming, I., Fouroughi, P., Boctor, E., Hager, G., "*Ultrasound Elastography Mosaicing*", in Proceedings of Medical Image Computing and Computer Assisted Interventions (MICCAI)

With regards to **Task 1. Education and Training (Year 1-3)**, I am constantly learning and improving as a prostate cancer scientist. I have regular meetings with my mentors, Dr. Allaf, Dr. Macura and Dr. Boctor which provide me with urology and radiology insights. I have completed relevant coursework (*Surgical* Robotics, *Computer Integrated Surgery* Seminar) and also the education needed to prepare and propose to the IRB for human and animal studies (Human subject research, Animal safety, Radiation safety, Animal care and use, Research ethics, Privacy issues, Blood borne pathogens). The biggest gains were made however discussing the direction and means of accomplishing our study's goals. I spent valuable time with the Johns Hopkins Hospital Pathology department, where I have witnessed first hand both the macro pathology and the micro pathology processing of prostate specimens. The pathology staff and doctors provided me with step by step directions through the process which was very helpful for developing a study in which ultrasound imaging would not hinder subsequent pathological processing. In preparing for the future animal study I also interacted with surgeons skilled in radical prostatectomy. These discussions, coupled with operating room observations with Dr. Allaf and Dr. Su are the foundation of my prostate cancer education and training. With respect to my engineering education and training, I have completed all the courses recommended by my mentors but I continue to learn by participating in departmental and surgical robotics specific seminars, in which I am enrolled every semester. In 2012, I attended the SPIE Medical Imaging Conference which provided me with insight into the frequent collaborations between engineers and physicians.

3. KEY RESEARCH ACCOMPLISHMENTS

- Completion of study on *ex-vivo* prostate specimens using standard ultrasound probe as an equivalent to the LAPUS probe
- Analysis of study data; results show elastography has the potential to detect prostate cancer through direct interrogation techniques
- Phantom study using a modified prostate elastography phantom; comparison of LAPUS and TRUS; results show feasibility in lesion detection with elastography but there are concerns about probe manipulation due to its size
- Planning animal study to better evaluate usability and performance of LAPUS probe.

4. REPORTABLE OUTCOMES

1. Fleming, I., Rivaz, H., Boctor, E., Hager, G. "*Robust Dynamic Programming Method for Ultrasound Elastography*", Proceedings of SPIE Medical Imaging, San Diego, CA, February 2012 - published paper
2. Fleming, I., Rivaz, H., Boctor, E., Hager, G. "*Robust Dynamic Programming Method for Ultrasound Elastography*", Proceedings of SPIE Medical Imaging, San Diego, CA, February 2012 - presented poster.
3. Billings, S., Nishikant, D., Kang, H. J., Taylor, R., Boctor, E., "*System for robot-assisted real-time laparoscopic ultrasound elastography*," Proceedings of SPIE Medical Imaging, San Diego, CA, February 2012 - published paper.
4. Fleming, I., Kut, C., Macura, K., Su, L.-M., Rivaz, H., Schneider, C., Hamper, U., Lotan, T., Taylor, R., Hager, G., Boctor, E., " *Ultrasound elastography as a tool for imaging guidance during prostatectomy: Initial experience*", Med Sci Monit, 2012; 18(9)
5. Fleming, I., Fouroughi, P., Boctor, E., Hager, G., " *Ultrasound Elastography Mosaicing*", not published yet.

5. CONCLUSION

Ex-vivo prostate specimens study was completed using standard ultrasound probe as an equivalent to the LAPUS probe. Data was analyzed and the results show elastography has the potential to detect prostate cancer through direct interrogation techniques. Scientific findings were published in the Medical Science Monitor Journal. A phantom study using a modified prostate elastography phantom was completed. LAPUS and TRUS probe were compared and the results show feasibility in lesion detection with elastography but there are concerns about probe manipulation due to its size. An animal study to better evaluate usability and performance of LAPUS probe is planned for the next 9 months. Clinical, prostate cancer and engineering education and training are on track.

6. APPENDICES

1. Fleming, I., Rivaz, H., Boctor, E., Hager, G. "*Robust Dynamic Programming Method for Ultrasound Elastography*", Proceedings of SPIE Medical Imaging, San Diego, CA, February 2012 - published paper
2. Fleming, I., Rivaz, H., Boctor, E., Hager, G. "*Robust Dynamic Programming Method for Ultrasound Elastography*", Proceedings of SPIE Medical Imaging, San Diego, CA, February 2012 - presented poster.
3. Billings, S., Nishikant, D., Kang, H. J., Taylor, R., Boctor, E., "*System for robot-assisted real-time laparoscopic ultrasound elastography*," Proceedings of SPIE Medical Imaging, San Diego, CA, February 2012 - published paper.
4. Fleming, I., Kut, C., Macura, K., Su, L.-M., Rivaz, H., Schneider, C., Hamper, U., Lotan, T., Taylor, R., Hager, G., Boctor, E., " *Ultrasound elastography as a tool for imaging guidance during prostatectomy: Initial experience*", Med Sci Monit, 2012; 18(9)
5. Fleming, I., Fouroughi, P., Boctor, E., Hager, G., " *Ultrasound Elastography Mosaicing*", not published yet.

AD_____

Award Number: W81XWH-10-1-0562

TITLE: Improved Image-Guided Laparoscopic Prostatectomy

PRINCIPAL INVESTIGATOR: Ioana Fleming

CONTRACTING ORGANIZATION: The Johns Hopkins University
Baltimore, MD 21218

REPORT DATE: August 2012

TYPE OF REPORT: Annual Summary

PREPARED FOR: U.S. Army Medical Research and Materiel Command
Fort Detrick, Maryland 21702-5012

DISTRIBUTION STATEMENT: Approved for public release; distribution unlimited

The views, opinions and/or findings contained in this report are those of the author(s) and should not be construed as an official Department of the Army position, policy or decision unless so designated by other documentation.

REPORT DOCUMENTATION PAGE

Form Approved
OMB No. 0704-0188

Public reporting burden for this collection of information is estimated to average 1 hour per response, including the time for reviewing instructions, searching existing data sources, gathering and maintaining the data needed, and completing and reviewing this collection of information. Send comments regarding this burden estimate or any other aspect of this collection of information, including suggestions for reducing this burden to Department of Defense, Washington Headquarters Services, Directorate for Information Operations and Reports (0704-0188), 1215 Jefferson Davis Highway, Suite 1204, Arlington, VA 22202-4302. Respondents should be aware that notwithstanding any other provision of law, no person shall be subject to any penalty for failing to comply with a collection of information if it does not display a currently valid OMB control number. **PLEASE DO NOT RETURN YOUR FORM TO THE ABOVE ADDRESS.**

1. REPORT DATE *(DD-MM-YYYY)*	**2. REPORT TYPE**	**3. DATES COVERED** *(From - To)*

4. TITLE AND SUBTITLE	**5a. CONTRACT NUMBER**
	5b. GRANT NUMBER
	5c. PROGRAM ELEMENT NUMBER
6. AUTHOR(S) E-Mail:	**5d. PROJECT NUMBER**
	5e. TASK NUMBER
	5f. WORK UNIT NUMBER
7. PERFORMING ORGANIZATION NAME(S) AND ADDRESS(ES)	**8. PERFORMING ORGANIZATION REPORT NUMBER**
9. SPONSORING / MONITORING AGENCY NAME(S) AND ADDRESS(ES) U.S. Army Medical Research and Materiel Command Fort Detrick, Maryland 21702-5012	**10. SPONSOR/MONITOR'S ACRONYM(S)**
	11. SPONSOR/MONITOR'S REPORT NUMBER(S)

12. DISTRIBUTION / AVAILABILITY STATEMENT
Approved for Public Release; Distribution Unlimited

13. SUPPLEMENTARY NOTES

14. ABSTRACT

15. SUBJECT TERMS

16. SECURITY CLASSIFICATION OF:			**17. LIMITATION OF ABSTRACT**	**18. NUMBER OF PAGES**	**19a. NAME OF RESPONSIBLE PERSON**
a. REPORT	**b. ABSTRACT**	**c. THIS PAGE**			USAMRMC
U	U	U	UU		**19b. TELEPHONE NUMBER** *(include area code)*

Standard Form 298 (Rev. 8-98)
Prescribed by ANSI Std. Z39.18

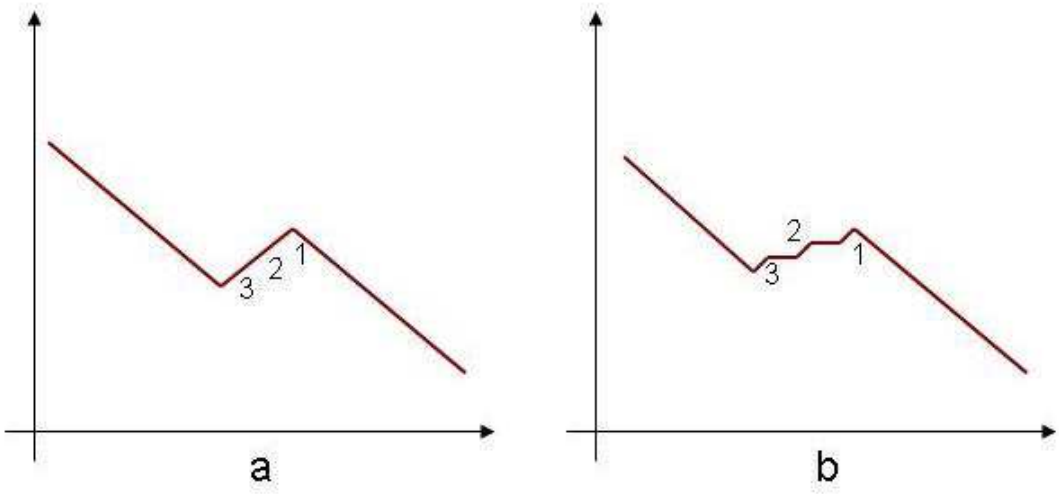

Figure 3. *Change-in-slope* detection algorithm. The 3 (three) positions where the change in slope is exhibited could be consecutive (a) or not (b)

4. RESULTS AND DISCUSSION

4.1 *Deformation Slope*

For a robust AM2D algorithm one single successful *seed* RF-line is sufficient. The *change-in-slope* parameter was designed to select good *seed* lines with monotonously increasing/decreasing displacement profile. Over all 1458 computations of the parameter (486 lines * 3 w values), the sensivity for selecting a good line was **91.7%**, while the specificity was **48.6%** (Table 2). The measure performed up to 93.1% sensitivity when tested across just one w value. We concluded the measure was promising but not sufficient on its own.

Table 2. *Change-in-Slope* (TP = true positive, FP = false positive, TN = true negative, FN = false negative)

		Prediction outcome		
		p	**n**	**total**
actual value	p′	TP = 835	FN = 238	P′
	n′	FP = 76	TN = 252	N′
	total	P	N	

4.2 *Displacement Stability*

486 scores were computed, one for each potential *seed* RF-line. The scores ranged from 0 to 0.2649. The average score for the good lines was 0.0058 (stdev = 0.0186) and the average score for the faulty lines was 0.0444 (stdev = 0.0586). A one-side Student t-test showed a **p-value** of $3.73909e-17$ (Table 3).

To increase the significance of the prediction value, we also computed a combined score for the two detection algorithms. The averaged *Change-in-Slope* score over the 3 (three) values for w was either 0, 0.33, 0.66, or 1, depending on how many of the three instances were deemed positive by the test. This score was added to the *Displacement Stability* score for a combined overall score. This overall score ranged from 0 to 1.1588. The average score for the good lines was 0.0795 (stdev = 0.2422) and the average score for the faulty lines was 0.4939 (stdev = 0.4444), for a **p-value** of $1.75837e-27$ (Table 3).

Table 3. Robustness score: Displacement Stability vs. Combined score for Displacement Stability + Change-in-Slope

	Displ. Stability		Displ. Stability + Change-in-Slope	
	Good Lines	Faulty Lines	Good Lines	Faulty Lines
Min	0	0	0	0
Max	0.1002	0.2649	1	1.1588
Avg	0.0058	0.0444	0.0795	0.4939
StDev	0.0186	0.0586	0.2422	0.4444
p-value	**3.73909E-17**		**1.75837E-27**	

Following the results of this analysis, a random search algorithm was implemented for the selection of a robust, stable *seed* RF-line as follows:

1. DP integer displacement is calculated for 5 random RF-lines, each at 5 random w values
2. A combined *Change-in-Slope* average plus *Displacement Stability* average score is computed
3. The most robust, stable line is chosen as the line with the smallest combined score, which also does not have any positive *Change-in-Slope* score
4. The chosen *seed* line's displacement values are propagated using the AM2D method

Given the current parallel computational resources, the addition of this selection test does not add a significant amount of time to the overall running time. DP takes the same time as before but it's now computed 25 times, and the computation of each score takes on the order of a couple of milliseconds. On 100 random runs of our testing algorithm, we only encountered 1 (one) situation where a faulty line was selected. The reason for the selection was that all 5 of the random line tested were faulty. This prompted us to introduce the additional condition that the chosen line should not have any positive *Change-in-Slope* score. Following this modification, no faulty situation has been encountered so far. We will continue to test our algorithm on the presented data set, as well as on new *ex-vivo* and *in-vivo* tissue data.

5. CONCLUSION

We proposed and successfully implemented an algorithm for the selection of a robust, stable RF-line to be used as *seed* for the DP displacement estimation and later propagated using the AM2D algorithm for elastography. The benefit of this algorithm is significant as it has the potential to improve the robustness of ultrasound elastography in *in-vivo* tissue which can be highly decorrelated. We are in the process of evaluating this hypothesis. The selection of robust *seed* RF-lines becomes even more important as we move towards real-time 3D ultrasound elastography.

REFERENCES

[1] J. Ophir, S. K. Alam, B. Garra, F. Kallel, E. Konofagou, T. Krouskop, T. Varghese, Elastography: ultrasonic estimation and imaging of the elastic properties of tissues, Proceedings of the Institution of Mechanical Engineers. Part H, Journal of Engineering in Medicine 213 (3) (1999) 203–233.

[2] H. Rivaz, E. Boctor, P. Foroughi, R. Zellars, G. Fichtinger, G. Hager, Ultrasound elastography: a dynamic programming approach, IEEE Transactions on Medical Imaging 27 (10) (2008) 1373–1377.

[3] J. Jiang, T. Hall, A regularized real-time motion tracking algorithm using dynamic programming for ultrasonic strain imaging, in: IEEE Ultrasonics Symp., Vancouver, Canada, 2006, pp. 606–609.

[4] H. Rivaz, E. M. Boctor, M. A. Choti, G. D. Hager, Real-time regularized ultrasound elastography, IEEE Transactions on Medical Imaging 30 (4) (2011) 928–945.

[5] G. Mase, Continuum Mechanics for Engineers, Third Edition (Computational Mechanics and Applied Analysis).

A Robust Dynamic Programming Method for Ultrasound Elastography

Ioana N. Fleming[1], Hassan Rivaz[1] , Emad M. Boctor[1,2] , and Gregory D. Hager[1]

[1] Johns Hopkins University, [2] Johns Hopkins Medical Institutions, Baltimore, MD, USA

ABSTRACT: *Ultrasound elastography is an imaging technology which can detect differences in tissue stiffness based on tissue deformation. For successful clinical use in cancer diagnosis and monitoring the method should be robust to sources of decorrelation between ultrasound images. A regularized Dynamic Programming (DP) approach was used for displacement estimation in compressed tissue. In the Analytic Minimization (AM) extension of DP, integer displacements are calculated just for one RF-line, and later propagated laterally throughout the entire image. This makes the seed RF-line very important; faulty seed lines could propagate erroneous displacement values throughout the image resulting in the appearance of false "lesions". In this paper we analyze the robustness of this method in free-hand palpation of laboratory tissue phantoms. An update to the algorithm includes a random search for the most robust seed RF-line. Axial integer displacements are obtained for 5 random lines individually with DP optimization. For each random axial RF-line, multiple random values for decorrelation compensation are used in the displacement estimation. The displacement values are then compared and several metrics of stability and consistency are considered. A ranking is established and the line deemed most robust will become the seed line for displacement propagation, while also selecting the most stable value for decorrelation compensation. The random search can be achieved at no additional computational cost in a parallel implementation. The results indicate significant improvement in the robustness of the DP approach, while maintaining real-time computation of strain images.*

INTRODUCTION:

- Take one image before compression,
- Compress tissue and take second image,
- Compare images and calculate displacement (tissue motion) field,
- Calculate strain image from the motion field

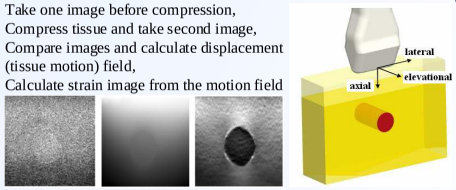

DYNAMIC PROGRAMMING (*DP*) + ANALYTIC MINIMIZATION (*AM*):

1. For images I_1 and I_2, calculate integer axial a_i and lateral l_i displacements of one seed RF-line using DP.
   - Displacement continuity term for line *j*:

$$R_j(a_i, l_i, a_{i-1}, l_{i-1}) = \alpha_a (a_i - a_{i-1})^2 + \alpha_l (l_i - l_{i-1})^2$$

   - Regularized cost function at the *i*th sample of the *j*th A-line:

$$C_j(a_i, l_i, i) = [I_1(i,j) - I_2(i + a_i, j + l_i)]^2 + \min_{d_a, d_l} \left\{ \frac{C_j(d_a, d_l, i-1) + C_{j-1}(d_a, d_l, i)}{2} + w R_j(a_i, l_i, d_a, d_l) \right\}$$

2. Calculate sub-sample axial and lateral displacements for the seed RF-line using 2D Analytic Minimization.
3. Propagate the solution of the seed RF-line to the left and right, using the displacement of the previous line as initial estimate.
   - Calculate a_i and l_i such as $(a_i + \Delta a_i,\ l_i + \Delta l_i)$ gives the axial and lateral displacements at the sample *i*. The regularized cost function becomes:

$$C_j(\Delta a_1, ..., \Delta a_m, \Delta l_1, ..., \Delta l_m) = \sum_m^{i=1} \{[I_1(i,j) - I_2(i + a_i + \Delta a_i, j + l_i + \Delta l_i)]^2 + \alpha (a_i + \Delta a_i - a_{i-1} - \Delta a_{i-1})^2 + \beta_a (l_i + \Delta l_i - l_{i-1} - \Delta l_{i-1})^2 + \beta_l' (l_i + \Delta l_i - l_{i,j-1})^2$$

, where α_a and α_l are axial and lateral regularization weights; *w* is a regularization weight for smoothness; α, β_a and β_l' are regularization terms which ensure continuity in displacements with respect to the top (axial α), and top - left/right (lateral β_l and β_l')

PROBLEM – Faulty *seed* RF-lines:

The displacement of the previous line will affect the displacement of the next line:
- bad initial estimate
- the last term → enforces lateral smoothness

For experimental evaluation we palpated a breast elastography phantom with a 10mm lesion and three times stiffer than the background. RF data was acquired with a 7.27MHz linear array at a sampling rate of 40MHz.
- Strain images using the AM-2D method, with each RF-line as a seed, each for 11 (eleven) values for *w* (smoothness regularization

w	Good Lines (%)	Faulty Lines (%)	Indeterminate (%)
0.10	44.2	55.8	-
0.15	57.8	42.2	-
0.20	61.3	33.6	5.1
0.25	68.1	30.0	1.9
0.30	65.0	30.5	4.5
0.35	61.7	32.0	5.3
0.40	53.3	41.8	4.9
0.45	53.1	46.9	-
0.50	43.4	56.6	-
0.55	32.1	67.9	-
0.60	24.3	75.8	-

Table 1: Percentage distribution of AM2D behavior for seed RF-lines given multiple values for *w* (smoothness regularization parameter)

***w* = (0.25, 0.35)** → high probability of finding a good *seed* RF-line

METHODS:

1. DEFORMATION SLOPE

Hypothesis: faulty lines would exhibit a perturbation in the monotonously decreasing slope of their displacement profile.

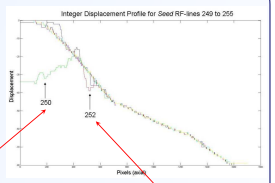

Figure 1: Integer DP displacement estimation for seed RF-lines 249 to 255. Note the areas (for lines 250 and 252 respectively) where the change in slope produces the artifact lesions

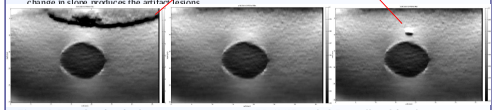

Figure 2. Examples of artifact lesions in strain images using DP AM2D method. Data collected from breast phantom freehand palpation.

A *change-in-slope* parameter was computed for the DP displacement profile for each seed RF-line, for w= 0:25; 0:30; 0:35.
486 lines were evaluated for each of the three values for w, for a total of **1458 computations**. Positive *change-in-slope* test: 3 or more positions exhibited a continuous change in the slope of displacement (Figure 3).

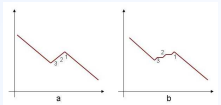

Figure 3: *Change-in-slope* detection algorithm. The 3 (three) positions where the change in slope is exhibited could be consecutive (a) or not (b)

		Prediction outcome		
		p	n	total
actual value	p'	TP = 835	FN = 238	P'
	n'	FP = 76	TN = 252	N'
	total	P	N	

Table 2: *Change-in-slope* predictor (TP = true positive, FP = false positive, TN = true negative, FN = false negative)

Sensitivity = 91.7%
Specificity = 48.6%

2. DISPLACEMENT STABILITY

Hypothesis: A robust seed RF-line will exhibit the same or similar DP displacement estimation across different *w* values.

Displacement Stability test: percentage of positions (pixels) where displacement values differ by more than 3 pixels for different values of *w*. For all 486 lines, 3 (three) pairs of displacement values were compared: 1) w = 0:25 vs. w = 0:30, 2) w = 0:30 vs. w = 0:35, 3) w = 0:25 vs. w = 0:35. Average the score for each line; final score between 0 and 1.

Combined score: the avg. *Change-in-Slope* score over the 3 values for *w* (0, 0.33, 0.66, or 1) was added to the

Table 3. Robustness score: Displacement Stability vs. Combined score for Displacement Stability + Change-in-Slope)

	Displ. Stability		Displ. Stability + Change-in-Slope	
	Good Lines	Faulty Lines	Good Lines	Faulty Lines
Min	0	0	0	0
Max	0.1002	0.2649	1	1.1588
Avg	0.0058	0.0444	0.0795	0.4939
StDev	0.0186	0.0586	0.2422	0.4444
p-value	3.73909E-17		1.75837E-27	

RESULTS:

MODIFIED DP + AM2D ALGORITHM

Select a robust, stable *seed* RF-line using random search:
1. DP integer displacement is calculated for 5 random RF-lines, each at 5 random *w* values;
2. A combined *Change-in-Slope* average plus *Displacement Stability* average score is computed;
3. The most robust, stable line is chosen as the line with the smallest combined score, which also does not have any positive *Change-in-Slope* score;
4. The chosen seed line's displacement values are propagated with AM2D.

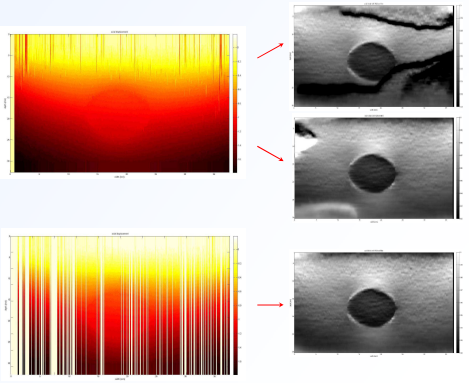

CONCLUSIONS:

We proposed and successfully implemented an algorithm for the selection of a robust, stable RF-line to be used as *seed* for the DP displacement estimation and later propagated using the AM2D algorithm for elastography. The benefit of this algorithm is significant as it has the potential to improve the robustness of ultrasound elastography in in-vivo tissue which can be highly decorrelated. The selection of robust seed RF-lines becomes even more important as we move towards real-time 3D ultrasound elastography.

REFERENCES:

[1] J. Ophir, et al, "Elastography: ultrasonic estimation and imaging of the elastic properties of tissues", Proceedings of the Institution of Mechanical Engineers. Part H, Journal of Engineering in Medicine 213 (3) (1999) 203-233.
[2] H. Rivaz, et al, "Ultrasound elastography: a dynamic programming approach", IEEE Trans Med Img 27 (10) (2008) 1373-1377.
[3] J. Jiang, T. Hall, "A regularized real-time motion tracking algorithm using dynamic programming for ultrasonic strain imaging", in: IEEE Ultrasonics Symp., Vancouver, Canada, 2006, pp. 606-609.
[4] H. Rivaz, et al, "Real-time regularized ultrasound elastography", IEEE Trans. on Medical Imaging 30 (4) (2011) 928-945.

Acknowledgements: Ioana Fleming is supported by the DOD Predoctoral Prostate Cancer Fellowship

System for Robot-Assisted Real-Time Laparoscopic Ultrasound Elastography

Seth Billings*[a], Nishikant Deshmukh[a], Hyun Jae Kang[a], Russell Taylor[a], Emad Boctor[ab]

[a]Dept. of Computer Science, Johns Hopkins University, 3400 N. Charles St., Baltimore, MD, USA 21218;

[b]Div. of Medical Imaging Physics, Johns Hopkins Medicine, 600 N. Wolfe St., Baltimore, MD, USA 21287

ABSTRACT

Surgical robots provide many advantages for surgery, including minimal invasiveness, precise motion, high dexterity, and crisp stereovision. One limitation of current robotic procedures, compared to open surgery, is the loss of haptic information for such purposes as palpation, which can be very important in minimally invasive tumor resection. Numerous studies have reported the use of real-time ultrasound elastography, in conjunction with conventional B-mode ultrasound, to differentiate malignant from benign lesions. Several groups (including our own) have reported integration of ultrasound with the daVinci robot, and ultrasound elastography is a very promising image guidance method for robot-assisted procedures that will further enable the role of robots in interventions where precise knowledge of sub-surface anatomical features is crucial. In this paper, we present a novel robot-assisted real-time ultrasound elastography system for minimally invasive robot-assisted interventions. Our system combines a daVinci surgical robot with an experimental software interface, a robotically articulated laparoscopic ultrasound probe, and our GPU-based elastography system. Elastography and B-mode ultrasound images are displayed as picture-in-picture overlays in the daVinci console. Our system minimizes dependence on human performance factors by incorporating computer-assisted motion control that automatically generates the tissue palpation required for elastography imaging, while leaving high-level control in the hands of the user. In addition to ensuring consistent strain imaging, the elastography assistance mode avoids the cognitive burden of tedious manual palpation. Preliminary tests of the system with an elasticity phantom demonstrate the ability to differentiate simulated lesions of varied stiffness and clearly delineate lesion boundaries.

DESCRIPTION OF PurPOSE / NEW WORK PRESENTED

Surgical robots provide many advantages for surgery, including minimal invasiveness, precise motion, high dexterity, and crisp stereovision. One limitation of current robotic procedures, compared to open surgery, is the loss of haptic information for such purposes as palpation, which can be very important in minimally invasive tumor resection. Numerous studies have reported the use of real-time ultrasound elastography, in conjunction with conventional B-mode ultrasound, to differentiate malignant from benign lesions in prostate, breast, pancreas, lymph nodes, and thyroid.[1,2,3,4,5] Ultrasound elastography is thus a very promising image guidance method for robot-assisted procedures that will further enable the role of robots in interventions where precise knowledge of hidden anatomical features is crucial. Several groups (including our own) have reported integration of ultrasound with the daVinci robot.[6,7,8] In this paper, we present a novel robot-assisted real-time ultrasound elastography system for minimally invasive robot-assisted interventions.

METHODS

In general, cancerous tissue has higher cell density than surrounding healthy tissue, which leads to elevated tumor stiffness that can be visualized using elastography techniques. As first described by Ophir et al.,[9] the principle of ultrasound elastography is to estimate tissue stiffness from measurement of tissue strain induced by an applied force. This is accomplished by measuring relative tissue displacements between ultrasound image pairs under different states of induced compression. Because ultrasound elastography algorithms assume an axial compression, strain image quality may degrade when non-axial motion or probe rotation occurs during compression. Axial compression is typically on the order of only a millimeter or two, and even small amounts of unwanted motion may affect image quality. Due to the variability in manual compression, image quality for free-hand elastography is highly dependent on practitioner skill and experience.

The quality of elastography imaging as a function of human performance is minimized by our robot-assisted elastography system through computer-integrated motion control for tissue compression, whereby tissue is autonomously compressed along the direction axial to the ultrasound probe. The system computer provides assistive

control of robot motion by generating a sinusoidal palpation motion that is overlaid onto motion commands from the master manipulators (**Error! Reference source not found.**). By this method, the surgeon retains overall control of the ultrasound probe position and orientation, while the computer controls the finer points of tissue compression. Because the computer has accurate knowledge of the ultrasound probe position and is not subject to motion errors like a human operator, consistent tissue compression in the precise axial direction is ensured.

The elastography assistance mode improves the precision and consistency of tissue compression beyond what can be achieved by manually controlled teleoperation while also reducing the cognitive burden for the user. Continual palpation of tissue under manual control is a tedious task imposing a large cognitive burden and demand of focus. By relieving this burden through computer assistance, the user is able to focus on more important tasks such interpreting real-time imaging information and conducting surgery.

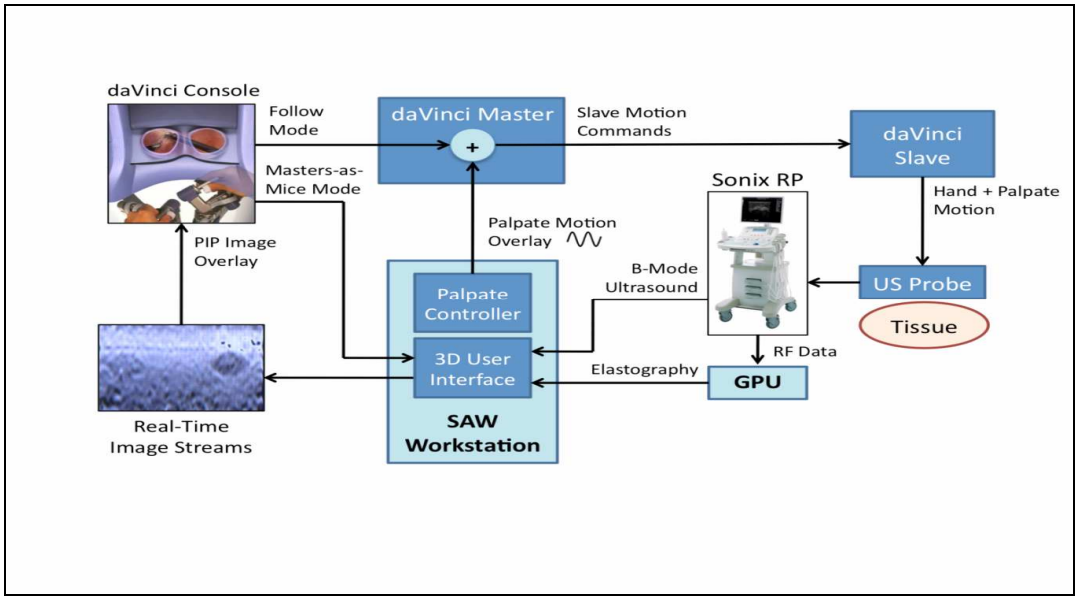

Figure 1. Block diagram of our robot-assisted system for real-time ultrasound elastography.

Error! Reference source not found. shows a block diagram of our complete system for robot-assisted ultrasound elastography. At the heart of the system is the daVinci S surgical robot (Intuitive Surgical Inc., Sunnyvale, CA). Computer integrated control of robot motion is facilitated by an experimental "Read/Write" Research Application Programming Interface (API) provided by Intuitive Surgical Inc., which enables robot motion to be controlled from computer in addition to control inputs from the master console, as discussed below. The daVinci robot manipulates a prototype version of a robotically articulated laparoscopic ultrasound probe (Figure 2a), also developed by Intuitive Surgical Inc., which was built into the form factor of a standard daVinci tool. The ultrasound probe has a linear array transducer (Gore, Newark DE) with 128 elements that measures 50mm in length with a probe diameter of approximately 9mm. The ultrasound probe is driven by a Sonix RP ultrasound system (Ultrasonix Medical Corp., Richmond BC Canada), which provides an Ultrasound Research Interface granting access to pre-beam formed RF data from the ultrasound probe. Access to this RF data is critical to reaching optimal performance from elastography algorithms. The RF data is processed by a high-performance external NVIDIA Tesla series GPU, which connects locally to the Sonix RP system. The GPU provides sufficient parallel computing power to generate strain images from RF data in real time using an elastography algorithm based on normalized cross-correlation.[10] The elastography images from the GPU are streamed from the Sonix RP system to a network port on the system's central workstation. The workstation also receives a parallel stream of conventional B-mode ultrasound images from the Sonix RP machine directly. The workstation sends both image streams to picture-in-picture overlays shown in the stereo display of the daVinci console. The picture overlays enable the surgeon to observe the ultrasound and elastography image feeds in real-time without releasing control of the robot arms or diverting attention away from the task at hand.

In collaboration with Intuitive Surgical, the Engineering Research Center for Computer-Integrated Surgical Systems and Technology (CISST ERC) at Johns Hopkins University has developed an open-source software framework for

medical robotics and computer assisted surgical systems research, which we call Surgical Assistant Workstation (SAW).[11,12,13,14] This open-source framework is an extension of the CISST software libraries developed at Johns Hopkins to enable rapid application development by providing capabilities including basic mathematics and numerical routines, thread execution management, inter-process communication, construction and control of video pipelines, and many other things.[15,16,17,18] Although the software components providing its basic capabilities are all open-source, SAW is designed to be compatible with proprietary modules through module wrappers using well-defined interface protocols. In particular, we have developed SAW wrappers that provide the ability to interface with the read-only and read-write research interfaces of the daVinci robot. The capabilities of the Read-Only daVinci Research Interface include the ability to query the state of the master and slave robot arms and of user console events.[14] The Read/Write daVinci Research Interface extends these features with the capability to use software to command motions of the master and slave robot arms and to trigger user events. One such feature allows us to superimpose an externally computed motion onto motion inputs from the master manipulators. We use this capability in our system to create computer generated motion overlays for tissue palpation. Another function of SAW allows us to use a master arm controller effectively as a 3D mouse. We call this masters-as-mice mode. We use this mode in our system to build an interactive environment for the daVinci operator to control and interact with video overlays.

The SAW software package is implemented on the central workstation of our system, which centralizes processing for user interaction with image overlays, acquisition of real-time image streams, and implementation of the control loop generating assistive motion for tissue palpation. A command terminal on the central workstation allows the user to set the amplitude and frequency of tissue palpation. These settings may be updated in real-time. The terminal also allows palpation to be activated/deactivated at will. The user interacts with the image overlays from the daVinci console using the SAW masters-as-mice mode, which, for the daVinci system, is activated by engaging the clutch foot pedal followed by a double-pinch of both master manipulators in unison. The masters-as-mice mode activates an interactive menu environment in which the daVinci master controllers manipulate virtual cursors in the daVinci console's stereo display (Figure 2a). Menu selections are made by moving a cursor to a menu icon and pinching the corresponding master controller. The elastography and B-mode ultrasound image overlays are activated by selecting the appropriate menu icon with a virtual cursor (pinching master controller selects). The image overlays are resized and repositioned in the daVinci display by dragging them with a cursor. Releasing the clutch pedal returns the master manipulators to control of the slave arms and maintains the image overlays in the user's field of view.

Results

Preliminary tests of the system have been conducted with a CIRS Model 049 Elasticity QA Phantom, which has simulated lesions of different calibrated stiffness. Figure 2b presents a snap-shot of the daVinci display taken during phantom testing with image overlays displaying the real-time imaging results. The elastography image in this figure shows clear difference in contrast between a soft and hard lesion, with the hard lesion appearing darker in the image. This distinction cannot be made from the B-mode ultrasound image in this figure. The elastography image also establishes clear delineation of lesion boundaries, which would not be discernible from B-mode ultrasound in the case of isoechoic lesions. These images were recorded with tissue palpation set to 1mm amplitude and 1Hz frequency.

CONCLUSION

We have successfully implemented a robot-assisted system for minimally invasive, real-time ultrasound elastography. Our system provides an improvement over manual elastography techniques by unifying motion commands from a user with the precision and accuracy of computer-assisted motion control to ensure consistent and precise tissue strain. Our approach effectively reduces the cognitive load of the human operator while maintaining a user's control of the procedure. Preliminary tests using an elasticity phantom demonstrate the system's capability to generate strain images in real-time that can be used to delineate simulated lesion boundaries and differentiate lesions of varying stiffness.

Acknowledgements

Funding for this work was provided by Intuitive Surgical Research Grant, National Institutes of Health Individual Graduate Partnership Program (Clinical Center, Radiology & Imaging Sciences), and Johns Hopkins Internal Funds.

Significant background technology for this project was funded in part by NSF cooperative agreement EEC9731478 and by NIH Grants R41RR019159 and R42RR019159.

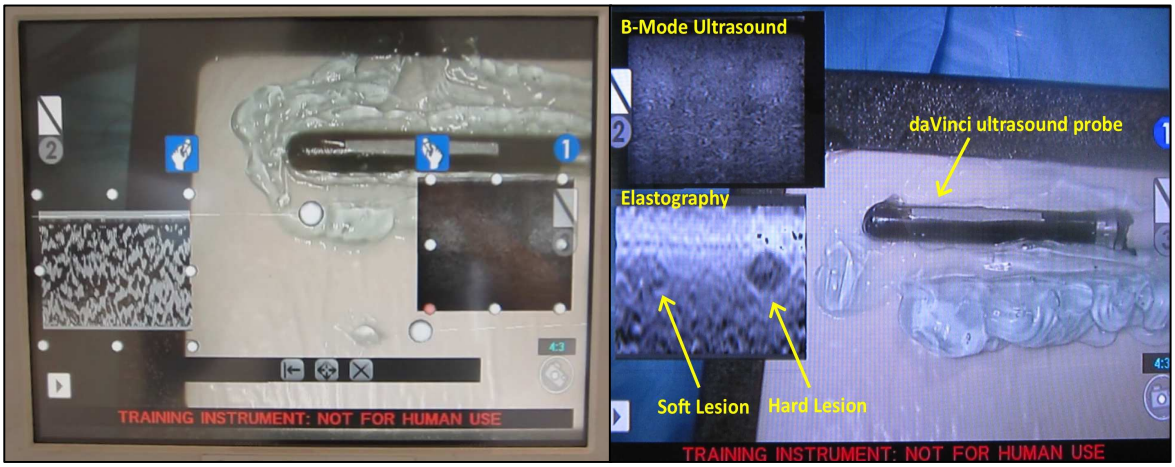

(a) (b)

Figure 2. a) Interactive menu environment for displaying image overlays in the daVinci console display, showing an active menu with two virtual mice corresponding to the left and right master manipulators and two picture-in-picture image overlays (picture taken of a patient side monitor). b) View of the daVinci console display during a test with an elasticity phantom; the elastography image overlay differentiates lesions of different stiffness.

THIS WORK HAS NOT BEEN SUBMITTED FOR PUBLICATION OR PRESENTATION ELSEWHERE.

REFERENCES

[1] Kamoi, K., Okihara, K., Ochiai, A., Ukimura, O., Mizutani, Y., Kawauchi, A., Miki, T., "The utility of transrectal real-time elastography in the diagnosis of prostate cancer," Ultrasound in Medicine & Biology 34(7), 1025-1032 (2008).

[2] Tan, S., Teh, H., Kent Mancer, J., and Poh, W., "Improving B mode ultrasound evaluation of breast lesions with real-time ultrasound elastography–A clinical approach," The Breast 17(3), 252-257 (2008).

[3] Hong, Y., Liu, X., Li, Z., Zhang, X., Chen, M., and Luo, Z., "Real-time ultrasound elastography in the differential diagnosis of benign and malignant thyroid nodules," J. Ultrasound Med. 28(7), 861-867 (2009).

[4] Saftoiu, A., Vilmann, P., Hassan, H., Gorunescu, F., "Analysis of endoscopic ultrasound elastography used for characterisation and differentiation of benign and malignant lymph nodes," Ultraschall in Med 27(6), 535-542 (2006).

[5] Saftoiu, A., Vilmann, P., Gorunescu, F., Gheonea, D., Gorunescu, M., Ciurea, T., Popescu, G., Iordache, A., Hassan, H., and Iordache, S., "Neural network analysis of dynamic sequences of EUS elastography used for the differential diagnosis of chronic pancreatitis and pancreatic cancer," Gastrointestinal Endoscopy 68(6), 1086-1094 (2008).

[6] Leven, J., Burschka, D., Kumar, R., Zhang, G., Blumenkranz, S., Dai, X., Awad, M., Hager, G., Marohn, M., Choti, M., Hasser, C., and Taylor, R., "DaVinci canvas: A telerobotic surgical system with integrated, robot-assisted, laparoscopic ultrasound capability", MICCAI 2005, LNCS Vol. 3749, 811-818 (2005).

[7] Schneider, C., Dachs, G., Hasser, C., Choti, M., DiMaio, S., and Taylor, R., "Robot-Assisted Laparoscopic Ultrasound," IPCAI 2010, LNCS Vol. 6135, 67-80 (2010).

[8] Schneider, C., Guerrero, J., Nguan, C., Rohling, R., and Salcudean, S., "Intra-operative "pick-up" ultrasound for robot assisted surgery with vessel extraction and registration: A feasibility study", IPCAI 2011, LNCS Vol. 6689, 122-132 (2011).

[9] Ophir, J., Cespedes, I., Ponnekanti, H., Yazdi, Y., and Li, X., "Elastography: A quantitative method for imaging the elasticity of biological tissues", Ultrasonic Imaging 13(2), 111-134 (1991).

[10] Deshmukh, N., Rivaz, H., and Boctor, E., "GPU-based elasticity imaging algorithms", Proc. Int. Conf. Med. Imag. Comp. & Comp. Assist. Interven., (2009).

[11] Jung, M., Deguet, A., and Kazanzides, P., "A component-based architecture for flexible integration of robotic systems", IROS 2010, 6107-6112 (2010).

[12] Jung, M., Xia, T., Deguet, A., Kumar, R., Taylor, R., and Kazanzides, P., "A Surgical Assistant Workstation (SAW) application for teleoperated surgical robot system", Sys. & Arch. for Comp. Assist. Interven., Midas Journal, (2009).

[13] Balazs, V., Simon, D., Anton, D., Peter, K., Rajesh, K., Christopher, H., and Russell, T., "The Surgical Assistant Workstation", MICCAI 2008 Workshop, Midas Journal, (2008).

[14] DiMaio, S. and Hasser, C., "The da Vinci research interface", MICCAI 2008 Workshop, Midas Journal, (2008).

[15] Kazanzides, P., Deguet, A., Kapoor, A., "An architecture for safe and efficient multi-threaded robot software", TePRA 2008, 89-93 (2008).

[16] Deguet, A., Kumar, R., Taylor, R., and Kazanzides, P., "The cisst libraries for computer assisted intervention systems", MICCAI 2008 Workshop, Midas Journal, (2008).

[17] Kapoor, A., Deguet, A., Kazanzides, P., "Software components and frameworks for medical robot control," ICRA 2006, 3813-3818 (2006).

[18] Kazanzides, P., Deguet, A., Kapoor, A., Sadowsky, O., LaMora, A., and Taylor, R., “Development of open source software for computer-assisted intervention systems”, 2005 MICCAI Open-Source Workshop, Insight Journal, (2005).

© Med Sci Monit, 2012; 18(9): CR
PMID: XXXXXXXX

WWW.MEDSCIMONIT.COM
Clinical Research

CR

Received: 2011.XX.XX
Accepted: 2011.XX.XX
Published: 2012.XX.XX

Ultrasound elastography as a tool for imaging guidance during prostatectomy: Initial experience

Authors' Contribution:
A Study Design
B Data Collection
C Statistical Analysis
D Data Interpretation
E Manuscript Preparation
F Literature Search
G Funds Collection

Ioana Nicolaescu Fleming[1ABCDEF], Carmen Kut[1,2ABCDF], Katarzina Macura[2ABDEG], Li-Ming Su[3ABD], Hassan Rivaz[1ABC], Caitlin Schneider[1ABC], Ulrike Hamper[2D], Tamara Lotan[2C], Russ Taylor[1ADG], Gregory Hager[1ADG], Emad Boctor[1,2ABDEG]

[1] Johns Hopkins University, Baltimore, MD, U.S.A.
[2] Johns Hopkins University School of Medicine, Baltimore, MD, U.S.A.
[3] Department of Urology, University of Florida College of Medicine, Gainesville, FL, U.S.A.

Source of support: This work was supported by: NSF ERC grant EEC9731748, NIH grant 2R42RR019159, and NIH/NCI grant P50CA103175

Summary

Background: During laparoscopic or robotic assisted laparoscopic prostatectomy, the surgeon lacks tactile feedback which can help him tailor the size of the excision. Ultrasound elastography (USE) is an emerging imaging technology which maps the stiffness of tissue. In the paper we are evaluating USE as a palpation equivalent tool for intraoperative image guided robotic assisted laparoscopic prostatectomy.

Material/Methods: Two studies were performed: 1) A laparoscopic ultrasound probe was used in a comparative study of manual palpation versus USE in detecting tumor surrogates in synthetic and *ex-vivo* tissue phantoms; N=25 participants (students) were asked to provide the presence, size and depth of these simulated lesions, and 2) A standard ultrasound probe was used for the evaluation of USE on *ex-vivo* human prostate specimens (N=10 lesions in N=6 specimens) to differentiate hard versus soft lesions with pathology correlation. Results were validated by pathology findings, and also by *in-vivo* and *ex-vivo* MR imaging correlation.

Results: In the comparative study, USE displayed higher accuracy and specificity in tumor detection (sensitivity=84%, specificity=74%). Tumor diameters and depths were better estimated using USE versus with manual palpation. USE also proved consistent in identification of lesions in *ex-vivo* prostate specimens; hard and soft, malignant and benign, central and peripheral.

Conclusions: USE is a strong candidate for assisting surgeons by providing palpation equivalent evaluation of the tumor location, boundaries and extra-capsular extension. The results encourage us to pursue further testing in the robotic laparoscopic environment.

key words: **prostatectomy • laparoscopy • robotics • ultrasonography • elastography**

Full-text PDF: http://www.medscimonit.com/fulltxt.php?ICID=XXXXX17885

Word count: XXXX
Tables: 2
Figures: 7
References: 31

Author's address: Ioana Fleming, 112 Hackerman Hall, 3400 N. Charles Street, Baltimore, MD 21218, U.S.A., e-mail: inicola1@jhu.edu

PROOF © INTERNATIONAL SCIENTIFIC LITERATURE

PROOF © INTERNATIONAL SCIENTIFIC LITERATURE

Background

Prostate cancer is the second leading cause of cancer death and the most common cancer detected in men in the United States. An estimated 217,730 new cases of prostate cancer were diagnosed in the United States, and approximately 32,050 men died of prostate cancer during 2010 [1]. Radical Prostatectomy (RP) aims for complete cancer resection and has been shown to improve cancer survival [2]. Robotic-assisted laparoscopic prostatectomy (RALP) has recently emerged as an alternative to open and laparoscopic procedures. The daVinci Surgical System (Intuitive Surgical, Sunnyvale, CA) provides 3-D visualization, higher magnification, hand tremor elimination and refined dexterity by incorporating wristed instrumentation. From 250 robotic cases in the beginning (2001), the number has reached 73,000 in 2009 (86% of the 85,000 American men who had prostate cancer surgery) [3,4].

Initial experiences with the daVinci surgical system have been positive: short learning curve, limited blood loss, less post-operative pain, favorable complication rates, and short hospital stay [3–10]. Despite fewer perioperative complications and shorter hospital stay, a recent paper found patients were three times more likely to require salvage therapy [11]. One theoretical disadvantage with regards to robotic surgery is the lack of tactile feedback. In open RPs, the surgeon uses his fingers to feel the periphery of the prostate gland [12]. Without tactile feedback, a robotic surgeon is unable to appreciate differences in tissue texture or firmness and therefore may not be able to tailor precisely the extent of tissue excision around the prostate gland in efforts to eradicate all cancerous tissue. Inadvertently leaving residual cancer cells behind, called a positive surgical margin (PSM), is highly associated with cancer recurrence. PSM rates were initially higher in RALP than in the open procedure, but they have been shown to decrease with surgeon's experience and improved technique [9,11].

As manual palpation helps guide the surgeon in the open procedure, an equivalent real-time guiding tool is needed for robotic prostatectomy. Imaging modalities like MRI or CT are not feasible intraoperatively, nor do they possess the sensitivity or specificity for accurate detection and localization of prostate cancer. Transrectal ultrasound (TRUS) is routinely used in diagnosis, in conjunction with digital rectal examination (DRE) and biopsies [13]. One center used TRUS for real-time monitoring and guidance during Laparoscopic RP and reported technical feasibility and enhanced precision by decreased PSM rates [14,15]. TRUS was capable of imaging a substantial percent of nonpalpable prostate cancers. The authors recognized however, the limitations of TRUS guidance; it requires considerable prior expertise and tends to identify primarily hypoechoic lesions, which were just 47% of the cancer nodules studied [15]. Today's prostate cancer patients are more likely to present with echogenic or isoechoic lesions because aggressive screening techniques lead to a shift toward smaller, early-stage cancers [16,17]; classic B-mode gray-scale ultrasound alone cannot identify these lesions.

Ultrasound (US) Elastography (USE) is emerging as a valuable tool in the field of imaging. Elastography is a qualitative technique based on the principle that tissue compression produces strain (displacement) within that tissue; strain is smaller in harder, stiffer tissue than in softer, more compliant tissue [18]. Analyzing the ultrasound raw radio frequency signal results in a strain map, commonly called *elastogram*, where harder tissue is darker than surrounding soft tissue. Cancers tend to present as hard lesions due to increased cellularity [18]. Echogenicity and stiffness of tissue are generally uncorrelated; USE can identify hypoechoic lesions, but also echogenic or isoechoic cancers that classic gray-scale ultrasonography cannot. Elastography through the transrectal approach has already been proven feasible in guiding biopsies of the prostate [19–22]. Integrating USE technology with a laparoscopic ultrasound probe will give robotic and laparoscopic surgeons an important image-guidance tool, which until this point does not exist [23–25].

This paper describes two experiments and results of an ongoing study evaluating the diagnostic accuracy and efficacy of using USE to identify the cancerous nodules in the prostate gland. The aim of the first study was to compare the ability of subjects to detect hard tissue (tumor surrogates) in synthetic and *ex-vivo* phantoms. We attempted to mimic an OR setting of open *vs.* robotic procedures, by asking the subjects to identify properties of the tissue using manual palpation in one arm, versus using ultrasound elastograms in the other arm. The elastograms were obtained with a laparoscopic ultrasound probe. In the second study, human *ex-vivo* prostatectomy specimens where used to assess the accuracy of USE in the identification and characterization of hard cancerous nodules. We compared the elastogram results with histopathology maps (the gold standard) and also to pre- and post-operative MR scans of the prostate gland in order to assess and co-localize anatomically USE with the reference histopathology and MR scans.

Material and Methods

Comparative study for USE *vs.* manual palpation in tumor detection

Institutional Review Board approval was obtained for the comparative study. We recruited N=25 local students to asses human ability to feel hard lesions through palpation, versus elastography's ability to distinguish the same lesions. Our decision to use local students instead of seasoned surgeons stemmed from the rationale that all humans are born with the sense of touch and thus have the innate sensory ability to palpate; we were also able to recruit more subjects in order to assess inter-observer variability. Participants were asked to identify lesions present in both synthetic and *ex-vivo* phantoms. The subjects evaluated the phantoms using manual palpation and ultrasound based elastograms. The hypothesis of the study was that subjects could identify lesions easier on the elastograms versus using manual palpation. Seven synthetic and four *ex-vivo* tissue phantoms were created. The phantoms mimicked the mechanical properties of prostate tissue and the acoustic scattering properties of human tissue. *Synthetic phantoms* exhibited deeper spherical hard lesions, consistent with deeper prostatic cancerous nodules, while *Ex-vivo phantoms* had superficial, free-form ablated lesions, more consistent with extra-capsular cancer extension.

Synthetic phantoms (3×2×2 inches) were made from Liquid Plastic (M-F Manufacturing Co., Inc., Haltom City, TX) and

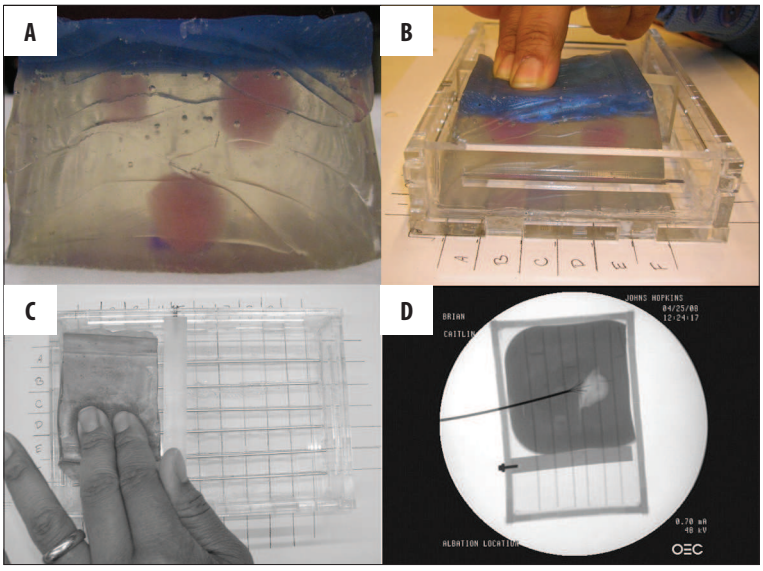

Figure 1. Synthetic phantoms: (**A**) lesions are visible from the side (pink) and the top is opaque (dark blue); (**B,C**) inside the grid calibration container; (**D**) X-ray of *ex-vivo* chicken phantom. Ablation probe, tines and the grid calibration container are visible.

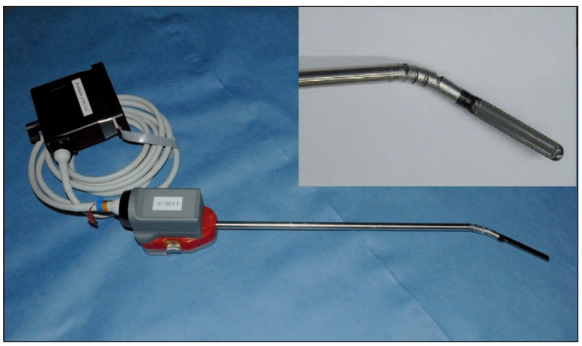

Figure 2. Laparoscopic ultrasound probe; close-up view of the probe's head (insert). Prototype courtesy of Intuitive Surgical.

glass micro-beads. The micro-beads were used as a scattering material. They were added to the plastic mix in an 1% concentration to mimic the acoustic scattering properties of human tissue; both the lesions and the rest of the phantom appeared isoechoic under B-mode ultrasound. Lesions were created by varying the mixing ratios of liquid plastic types; the ratio between 4116S Plastic Softener or 7116 Plastic Hardener and 8116 Super-Soft Plastic determined the final density and the elastic modulus of the lesions and the background [26]. Each phantom contained 0-3 harder spherical lesions (1-2 cm diameter) colored pink for ground truth identification (Figure 1A). The exposed top surface was colored opaque blue, to prevent the subjects from visually identifying the lesions (Figure 1A). The *synthetic phantoms* were sliced and sectioned at study end, following axial planes parallel with the ultrasound scanning plane. The depth of each lesion was measured as the distance between the surface of the phantom and the top of the lesion itself. The final depth of lesions for these 7 (seven) phantoms was measured to be between 7 and 25 mm.

Ex-vivo phantoms were constructed from raw chicken breast tissue. Hard lesions of various diameters were created using radio frequency (RF) ablation, at an average temperature of 95 degrees Fahrenheit for 20 minutes. This formed a hard spherical lesion at a depth of 1–6 mm below the surface, which allowed for possible palpation but not the visual localization of lesions. Before ablation, each tissue was placed in a small plastic container and surrounded by 150 Bloom porcine gelatin (Bloom represents an unit of measure for rigidity of gelatin). X-ray axial scans (projection plane parallel with the ultrasound scanning plane) were used to localize and measure the lesions (Figure 1D). The tissue phantoms were sliced on the same axial plane at study end to determine the depth and extent of the ablated areas. The depth of each lesion was measured as the distance between the surface of the phantom and the top of the lesion itself. For *ex-vivo* lesions, the final depth of lesions was measured to be less than 7 mm.

Hardware and software specification

For the comparative study, a laparoscopic ultrasound probe was used, fitted with a transducer (Gore Tetrad, Englewood, CO) with a center frequency of 7.5 MHz, and 128 elements (Figure 2) [23–25]. Ultrasound raw radio-frequency data was acquired using an Ultrasonix US scanner (Ultrasonix Medical Corporation, Richmond, BC, Canada). Due to the relative inexperience of our subjects, it was not possible to have the subjects perform real-time elastography. Thus, to maintain consistent image quality and to minimize user dependence, elastography images were obtained in a standardized manner by one of our researchers, prior to the evaluation. Elastograms were generated using the corresponding radio frequency data and our dynamic programming (DP) elastography algorithm [27,28].

During the study, each subject reviewed 3–4 phantoms, each placed in a self-designed calibration container, which consisted of a 5-by-5 grid, 0.5 inches apart, labeled with numbers and letters along the two axis (Figure 1B, C). Subjects were asked to identify by manual palpation the location based on the provided grid (i.e. B4 or A3), and also the diameter and depth of each lesion using 0.5 inches as the unit of reference. For the USE arm of the study, the subjects first underwent an USE training session, where they were explained the concept and shown sample elastograms. They were then presented with 3–4 elastograms of the phantoms and they were asked to provide the presence, size and depth of lesions given the scale of the images. The order in

PROOF © INTERNATIONAL SCIENTIFIC LITERATURE

PROOF © INTERNATIONAL SCIENTIFIC LITERATURE

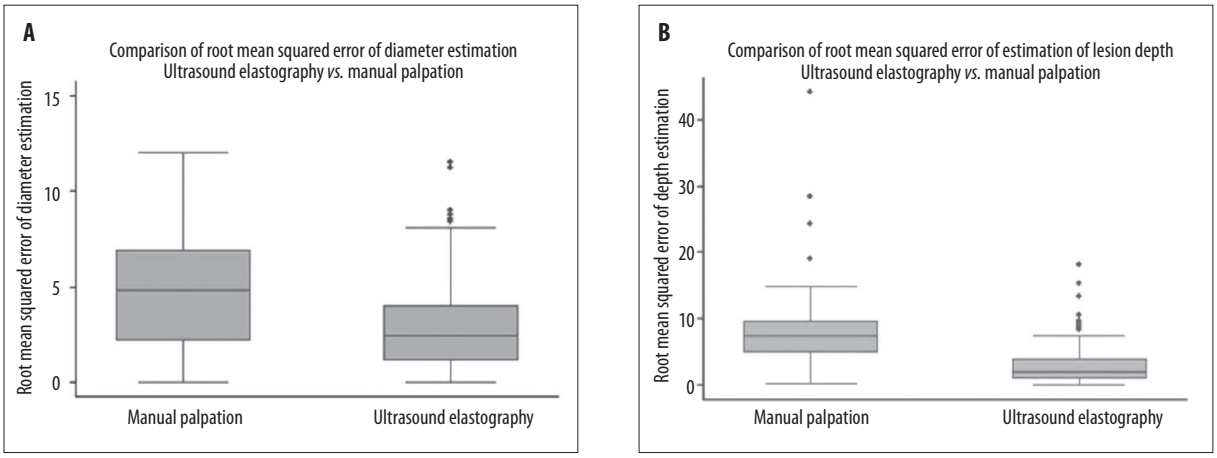

Figure 3. Synthetic phantom study results: Box-and-whisker plots for lesion diameter and depth from surface (**A,B**), and lesion detection rate according to depth (**C**).

which the subjects completed the USE and manual palpation tasks was randomized.

Accuracy was determined descriptively using box and whiskers plots (Figure 3A,B), sensitivity and specificity calculations, and root mean squared error of estimation (RMSE) obtained from subtracting the estimated value of the measured parameter (diameter, depth) from the ground truth value determined from direct measurement. STATA 9 (StataCorp LP, College Station, TX) was used to perform the statistical analysis, which consisted of Student's t-test for comparison between the means of the RMSE of both diameter and depth as estimated via manual palpation versus USE. The p-values reported were generated by t-test calculations assuming unequal variances for a two-tailed test where p=0.05.

Ex-vivo human prostate study for tumor detection

Prostate cancer patients, candidates for prostatectomy, were prospectively enrolled in our study, following an informed consent approved by the Institutional Review Board. The objective of the study was to evaluate the efficacy of using elastography to identify and precisely localize hard nodules such as seen with prostate cancer just beneath the surface of the prostate gland in the peripheral zone. In this area, cancerous lesions are at most risk of invasion beyond the confines of the prostate gland and also more likely to be cut across by a well meaning surgeon. We recruited patients who underwent both open and assisted prostatectomies given that the process of removing the gland was not a focus of our study. Patients underwent multiple radiological procedures. 1) Pre-operative 3 Tesla MRI of the pelvis was performed right before the surgery procedure. 2) Post-operative ultra high-resolution MRI at 9.4 Tesla was performed on the excised prostate specimen to correlate the results to *in-vivo* pre-operative imaging. 3) USE was then performed on the prostate specimen by an experienced radiologist blinded to the surgeon's findings and to the pre-operative pathology report. The collected radio-frequency (RF) data was used offline to recreate classic B-mode grey-scale images, and also to compute elastograms showing the stiffness of the tissue scanned [27,28].

Pre-operative and post-operative MR scans were used for anatomical correlation with the computed elastograms. For

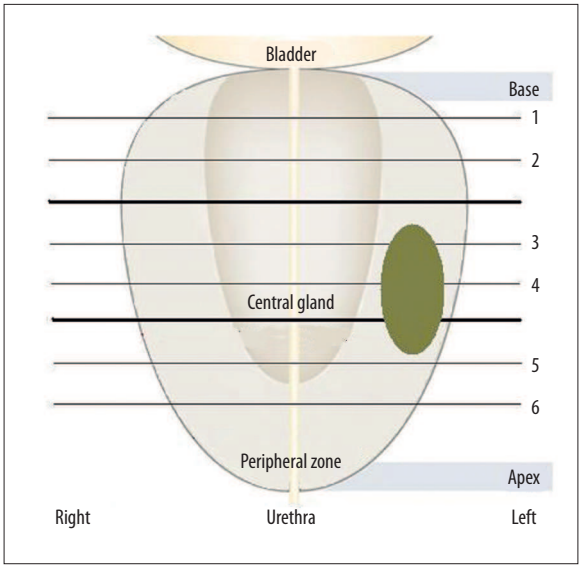

Figure 4. Ultrasound elastography data collection process using the sextant approach; RF data was acquired in axial planes (1–6) from the gland's base towards the apex. For illustration purposes, a lesion is outlined in the left mid section, peripheral zone of the specimen, similar with the case of specimen #3.

USE, the prostate specimens were placed in prone position on a surgical table. USE scans were performed in a systematic sextant approach, similar to that used for image guided biopsies. RF data was acquired in axial planes (from gland's base, through mid gland, to apex) on the left and right side of the gland (Figure 4). The sextant approach was necessary to ensure that the scans were in the same plane with the histopathology diagrams (axial) which constituted the gold standard for comparison. USE coronal scans from the left to the right of the gland were also performed; these scans were in alignment with the MR coronal scans.

Hardware and software specification

For the second study, USE acquisition was conducted using a Siemens Antares US scanner (Siemens Medical Solutions

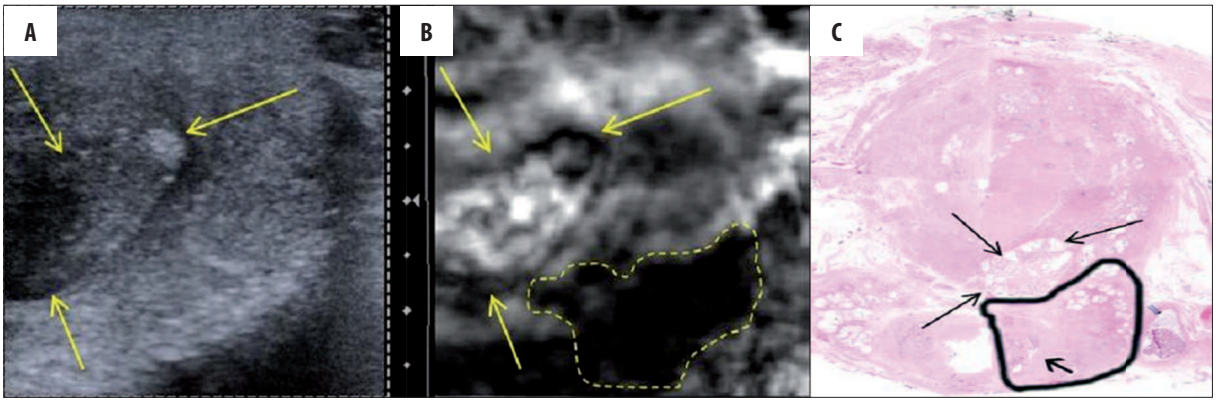

Figure 5. Axial section of prostate specimen #1 peripheral zone. Left lateral section of the prostate's base; classic ultrasound B-mode (**A**) and elastogram (**B**). Hard lesion is outlined, arrows point to adjacent nodule. (**C**) Hematoxylin & eosin stained histological section of prostate base. The tumor (Gleason score 3+5=8, outlined in black) extended beyond the prostatic capsule in this section and invaded the left seminal vesicle (arrow).

Table 1. Table summarizing the experimental results of the palpation study: sensitivity and specificity.

	Manual palpation	Ultrasound elastography
Sensitivity	66%	84%
Specificity	67%	71%
Detection rate <20 mm depth	80%	68%
Detection rate >20 mm depth	0%	66%
Detection rate	80%	84%

USA, Inc. Ultrasound Division, Issaquah, WA) with an ultrasound research interface to access raw RF data. Data was acquired by manual handling using a Siemens VF 10-5 linear array for prostate specimens. After RF data collection, elastograms were obtained using the dynamic programming (DP) elastography algorithm developed in our lab [27,28].

Each prostate specimen underwent routine pathologic processing and analysis. Due to the high volume of prostatectomies performed at our institution, the routine pathological process does not result in a whole mount mapping. Instead, for histopathological evaluation the prostatectomy specimens were initially sliced at every 3–4 mm from apex to base, according to the Stanford protocol. Each slice (6 to 10 master slices) were then incorporated in a paraffin block and sliced at 5 μ meter thickness. The slices were stained with hematoxylin-eosin and were then analyzed under a microscope by a pathologist blinded to the surgeon's findings and also to the elastography results. The localization and size of each tumor focus were documented for all step master slices on axial diagrams, with Gleason score. Large macro photographs were reconstructed in several specimens (Figure 5C). All data collected were stored in the database.

N=10 target areas were analyzed from N=6 patients enrolled so far into the elastography analysis. Histological findings served as the *gold standard* in determining the presence, location and size of any prostatic nodules, malignant and benign. The objective of our study was then to compare axial elastograms findings with the histological findings recorded by the pathologist (mapping diagrams, measurements and nodule characteristics such as malignant *vs.* benign). Since histopathology diagrams often specified just the maximum diameter of a lesion, coronal elastograms were used to better establish the location and extent of the identified lesions. MRI images (both axial and coronal planes) were aligned to the elastograms and provided help with their anatomical co-registration using anatomical details such as urethra or boundaries of peripheral zone *vs.* central gland.

Results

Comparative study for tumor detection

Overall sensitivity and specificity results are summarized in Table 1. USE showed higher accuracy in tumor detection with a sensitivity of 84% and specificity of 71%, compared to a sensitivity of 66% and a specificity of 67% for manual palpation. At depths greater than 20 mm, no subject was able to identify a lesion by manual palpation. 66% of these lesions were correctly identified on elastograms.

Diameter estimation for synthetic phantoms using manual palpation was less accurate than USE (p=0.001) with a root mean squared error of estimation (RMSE) of 4.81 for manual palpation (95% CI between 3.83 and 5.78), versus mean RMSE=3.02 for USE (95% CI between 2.57 and 3.47). For *ex-vivo* phantoms, estimations were comparable in both manual palpation and USE, at a RMSE of about 11.0 mm. Depth estimation for synthetic phantoms was statistically higher using manual palpation than USE (p=0.0001) with a mean value of the RMSE of 8.81 for manual palpation (95% CI between 6.24 and 11.39) versus a mean value of the RMSE=3.02 for USE (95% CI between 2.42 and 3.63) – Figure 4. For *ex-vivo* phantoms, estimations were comparable again for both manual palpation and USE, at a RMSE of about 1.0 mm.

Ex-vivo human prostate study

Elastography identified N=10 lesions, 8 hard nodules in the peripheral zone, 1 hard and 1 soft nodule in the central

PROOF © INTERNATIONAL SCIENTIFIC LITERATURE

Table 2. Prostate specimen data: A total of 10 (ten) elastography lesions were identified in 6 (six) patients' specimens (8 malignant and 2 benign).

#	Location	Gleason score	Size (cm)		
			Elastography	Pathology	MRI
1.1	PZ base	3+5	1.4×0.8	1.3×0.8	1.3×1.1
1.2	CG base	N/A-Solid	0.7×1.1	1.0×1.0	1.0×1.1
1.3	CG base	N/A-Soft	1.1×0.8	1.0×1.0	1.0×0.9
2.1	PZ base	5+3	3.0×1.3	2.4×1.0	2.0×1.5
3.1	PZ mid	4+5	2.4×0.8	1.9×1.0	1.5×1.2
4.1	PZ mid	3+3	1.0×0.5	0.5×0.4	0.6×0.7
4.2	PZ mid	3+4	1.5×0.9	1.1×0.5	1.1×0.8
5.1	PZ apex	3+3	0.5×0.6	0.5×0.5	0.6×0.6
5.2	PZ apex	4+3	0.6×1.0	0.8×0.9	0.9×0.9
6.1	PZ base	3+3	0.7×1.2	0.7×1.8	0.7×0.7

PZ – peripheral zone; CG – central gland.

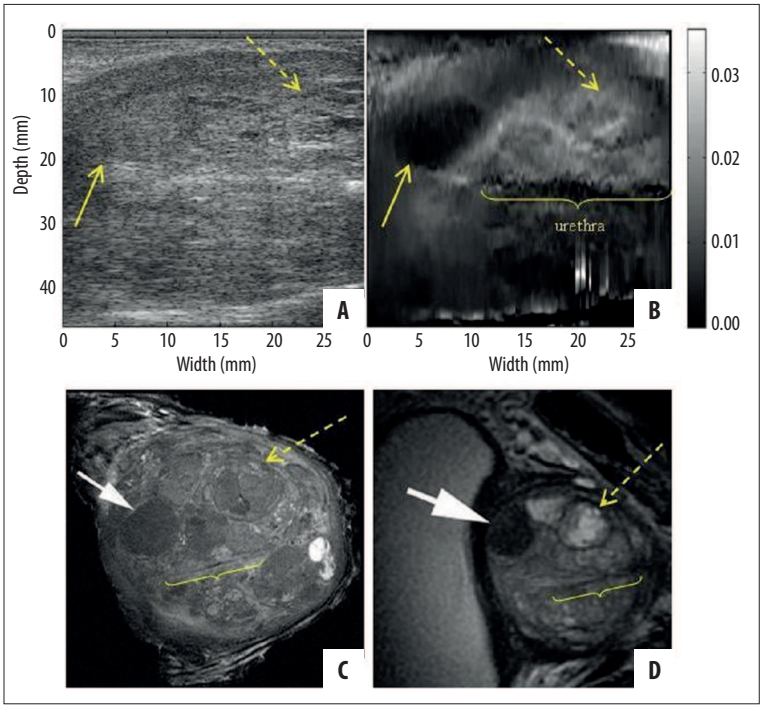

Figure 6. Coronal section of prostate specimen #1 at the level of the central gland. Classic ultrasound B-mode (**A**) and elastogram (**B**). 9.4 Tesla *ex-vivo* (**C**) and 3 Tesla *in-vivo* (**D**) MRI images are presented in coronal planes, in CCW (counter clock wise) orientation for better visualization of the correlation between USE and MRI of the specimen. Benign solid (arrow) and soft (dashed arrow) nodules and urethra are visible.

gland (Table 2). Pathology reports showed 8 of these lesions as malignant and 2 as benign. Diameter measurements correlation proved difficult because of the inability to perfectly register the three investigative modalities. USE and MRI measurements were within on average 2.05 mm *vs.* 2.25 mm of the diameters measured by pathology (standard deviation of 1.9 mm for USE and 2.9 mm for MRI). Size measurements and Gleason score are reported in Table 1.

Specimen #1 presented multiple hard and soft lesions, located in the central gland of the prostate (Figure 6). The *ex-vivo* T2-weighted coronal image from specimen MRI obtained at 9.4 Tesla (Figure 6C) – here in counter clock wise orientation for better visualization of the correlation between USE and MRI of the specimen) shows detailed anatomy of the heterogeneous central gland with a solid benign prostatic hypertrophy nodule (BPH) confirmed by pathology. Elastography was able to detect this solid nodule despite the heterogeneity of the prostate (Figure 6B) – solid arrow, whereas the lesion was not clearly identified by gray scale ultrasound. *Ex-vivo* T2-weighted 9.4 Tesla coronal image from specimen MRI also shows an additional soft cystic BPH nodule (dashed arrow). Urethra is also visible on the elastogram, as well as MRI exam (labeled *urethra*).

PROOF © INTERNATIONAL SCIENTIFIC LITERATURE

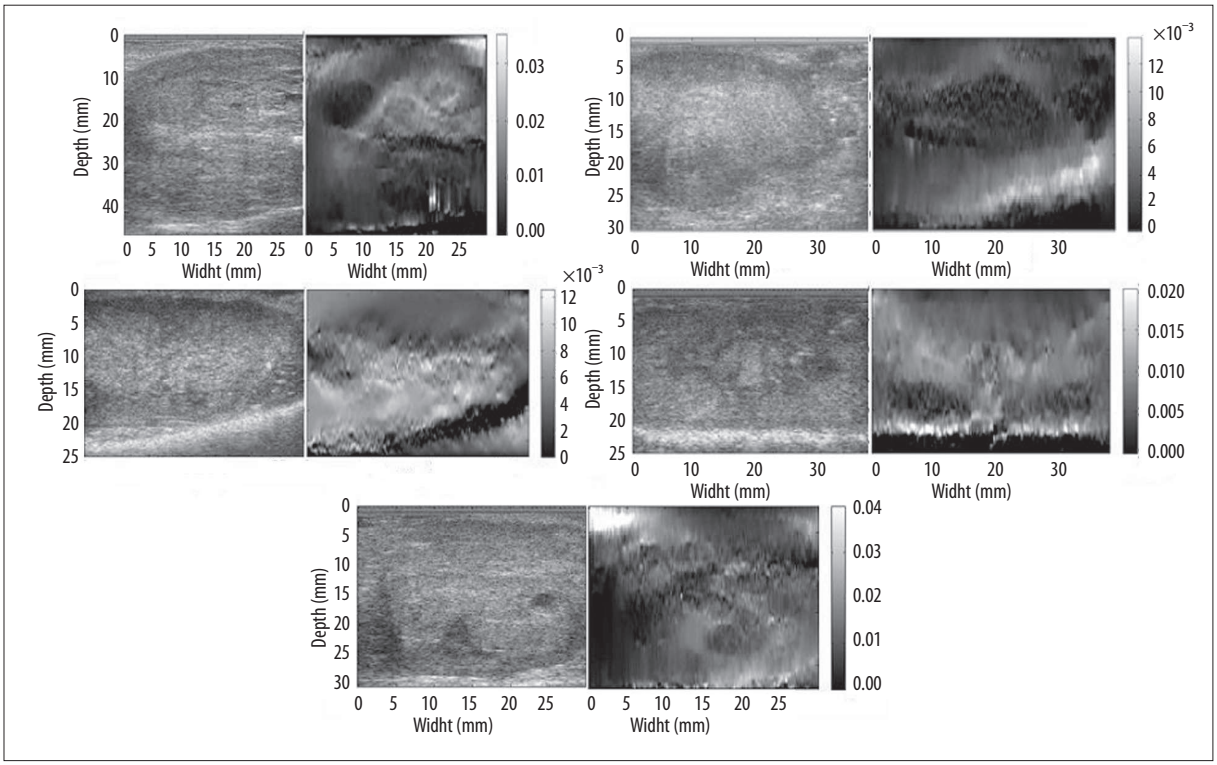

Figure 7. B-mode image (left) and elastogram (right) from specimens # 2–6. Dark regions at the very bottom of elastograms represent structures outside the prostate tissue (e.g. operating table). The border of the prostatic tissue can be easily noticed as a highly reflective band at the bottom of B-mode images.

Axial scans of the same specimens were compared with histopathology axial cross-sections. The prostate, submitted for histological processing in four quadrant sections per slice, was digitally realigned to reconstruct a full histological cross-section (Figure 5C). Specimen #1 was found with a tumor with Gleason score of 8 at the prostate base, left side (outlined). Figure 5A shows an ultrasound B-mode image and an elastogram obtained through an axial plane at the prostate's base on the left side. The same tumor was identified by elastography (Figure 5B – dashed contour) but is not visible on grey-scale ultrasound. For an anatomical correlation, a soft - cystic nodule anterior to cancer can be seen on B-mode image and USE (Figure 5A,B – arrows) and on histopathology (Figure 5C – arrows).

The remaining 5 (five) prostate specimens presented with superficial lesions in the peripheral zone of the gland. USE identified multiple hard malignant lesions in various locations, from the base to the apex of the prostate gland. One can notice the clear delimitations of these lesions on USE (Figure 7) as well as the close estimations of size versus pathology and MRI.

Discussion

In surgical procedures where manual palpation would be helpful but not possible to perform, e. g. laparoscopic robotic surgery, USE can offer added value if proven to be accurate in detecting pathologic lesions. Our comparative study showed USE to be superior to manual palpation in general sensitivity and specificity, and also in identifying deeper lesions. Despite of the inexperience of our subjects with USE and elastogram evaluation, USE demonstrated good performance in detection of hard lesions. This is particularly important as surgeons can be considered inexperienced elastogram readers as well. Our feasibility study showed that USE was able to identify both hard and soft lesions in the *ex-vivo* prostate specimens, located in the deep prostatic central gland and in the peripheral zone. Histopathologic findings validated USE, and results compared favorably with the *in-vivo* pre-surgical and *ex-vivo* post-surgical MRI scans. In the central gland of the prostate, elastography showed excellent detection of hard and soft areas, despite the complexity of the central gland. Elastography was able to identify both hard and soft BPH nodules and anatomical landmarks like the urethra (note excellent anatomical correlation to MR scan findings). In the peripheral zone USE identified multiple hard malignant lesions, from the base to the apex of the prostate gland. These preliminary results demonstrate the ability of USE to detect hard nodules in the prostate and are encouraging in the pursuit of this technology as a palpation equivalent imaging tool for prostatectomy.

USE maps tissue elasticity which makes it an ideal imaging modality to serve as a surrogate and possible equivalence to manual palpation in identifying hard cancerous tissue in the prostate gland, especially in the peripheral zone but also in the central gland. Real-time intra-operative imaging guidance is needed for identifying the presence of cancer within the prostate, especially near the capsule where tumor can invade and spread outside of the gland, and also for studying surrounding structures. If diseased hard lymph nodes could be detected, then lymphadenectomy may provide a more accurate cancer staging, help tailor future therapy,

PROOF © INTERNATIONAL SCIENTIFIC LITERATURE

PROOF © INTERNATIONAL SCIENTIFIC LITERATURE

and potentially prevent recurrence. A better delineation of the bladder neck and apex during dissection, especially when prostate cancer is located at the apex could perhaps improve patients' outcome. If deemed possible, imaging cavernous nerves (CNs) located along the immediate surface of the prostate gland may lead to their preservation, and thus improved preservation of potency and urinary continence [29]. Further more, the development of the elastography technology as an imaging guiding tool during prostatectomy could potentially be useful in the open procedures as well, where the manual palpation would not be enough to identify deeper lesions. It has been documented in the literature that prostate carcinoma originates in the central gland and transitional zone in up to 30% of cases [30,31].

Conclusions

Our initial experience showed USE was able to reliably identify hard nodules in the peripheral zone of the prostate that were prostate cancers. Additionally, USE showed its ability to define tissue hardness of BPH nodules despite the underlying tissue complexity in the central gland. Our comparative study demonstrated USE can approach the efficacy of manual palpation for superficial lesions and has the potential to surpass it for smaller, deeper lesions. We employed a laparoscopic ultrasound probe which was successfully used and tested in conjunction with elastography algorithms. Our initial experience with USE encourages us to pursue further the evaluation of this technique. Further testing of the laparoscopic probe is needed in a real laparoscopic environment. We can conclude that there is promise is integrating laparoscopic ultrasound elastography as a real-time, *in-vivo* imaging tool to guide surgeons during robotic-assisted prostatectomies.

Acknowledgements

We thank our colleagues, surgeon Mohammed Allaf and Naima Carter-Monroe, and also Intuitive Surgical for their help. Ioana Fleming is supported by the Department of Defense Prostate Cancer Predoctoral Fellowship.

References:

1. Jemal A, Siegel R, Xu J, Ward E: Cancer statistics, 2010. CA: A Cancer Journal for Clinicians. 2010; 60(5): 277–300
2. Bill-Axelson A, Holmberg L, Ruutu M et al: Radical prostatectomy versus watchful waiting in early prostate cancer. N Engl J Med, 2011; 364(18): 1708–17
3. Box GN, Ahlering TE: Robotic radical prostatectomy: long-term outcomes. Curr Opin Urol, 2008; 18(2): 173–79
4. Pruthi RS, Wallen EM: Current status of robotic prostatectomy: promises fulfilled. J Urol, 2009; 181(6): 2420–21
5. Nelson B, Kaufman M, Broughton G et al: Comparison of length of hospital stay between radical retropubic prostatectomy and robotic assisted laparoscopic prostatectomy. J Urol, 2007; 177(3): 929–31
6. Artibani W, Fracalanza S, Cavalleri S et al: Learning curve and preliminary experience with da Vinci-assisted laparoscopic radical prostatectomy. Urol Int, 2008; 80(3): 237–44
7. Colombo J, Jose R, Santos B et al: Robotic assisted radical prostatectomy: surgical techniques and outcomes. International Braz J Urol, 2007; 33(6): 803–9
8]. Badani KK, Kaul S, Menon M: Evolution of robotic radical prostatectomy: assessment after 2766 procedures. Cancer, 2007; 110(9): 1951–58
9. Ficarra V, Cavalleri S, Novara G et al: Evidence from robot-assisted laparoscopic radical prostatectomy: a systematic review. Eur Urol, 2007; 51(1): 45–55; discussion 56
10. Berryhill J Roy, Jhaveri J, Yadav R et al: Robotic prostatectomy: a review of outcomes compared with laparoscopic and open approaches. Urology, 2008; 72(1): 15–23
11. Hu JC, Wang Q, Pashos CL et al: Utilization and outcomes of minimally invasive radical prostatectomy. J Clin Oncol, 2008; 26(14): 2278–84
12. Walsh PC, Lepor H, Eggleston JC: Radical prostatectomy with preservation of sexual function: anatomical and pathological considerations. Prostate, 1983; 4(5): 473–85
13. Salomon G, Kllerman J, Thederan I et al: Evaluation of prostate cancer detection with ultrasound real-time elastography: a comparison with step section pathological analysis after radical prostatectomy. Eur Urol, 2008; 54(6): 1354–62
14. Ukimura O, Gill IS, Desai MM et al: Real-time transrectal ultrasonography during laparoscopic radical prostatectomy. J Urol, 2004; 172(1): 112–18
15. Ukimura O, Magi-Galluzzi C, Gill IS: Real-time transrectal ultrasound guidance during laparoscopic radical prostatectomy: impact on surgical margins. J Urol, 2006; 175(4): 1304–10
16. Coley CM, Barry MJ, Fleming C, Mulley AG: Early detection of prostate cancer. Part I: Prior probability and effectiveness of tests. Ann Intern Med, 1997; 126(5): 394–406
17. Daehnert WF, Hamper UM, Eggleston JC et al: Prostatic evaluation by transrectal sonography with histopathologic correlation: the echopenic appearance of early carcinoma. Radiology, 1986; 158(1): 97–102
18. Ophir J, Alam SK, Garra B et al: Elastography: ultrasonic estimation and imaging of the elastic properties of tissues. Proc Inst Mech Eng H, 1999; 213(3): 203–33
19. Cochlin DL, Ganatra RH, Griffiths DFR: Elastography in the detection of prostatic cancer. Clin Radiol, 2002; 57(11): 1014–20
20. Koenig K, Scheipers U, Pesavento A et al: Initial experiences with real-time elastography guided biopsies of the prostate. J Urol. 2005; 174(1): 115–17
21. Sumura M, Shigeno K, Hyuga T et al: Initial evaluation of prostate cancer with real-time elastography based on step-section pathologic analysis after radical prostatectomy: a preliminary study. Int J Urol, 2007; 14(9): 811–16
22. Leven J, Burschka D, Kumar R et al: DaVinci canvas: a telerobotic surgical system with integrated, robot-assisted, laparoscopic ultrasound capability. Med Image Comput Comput Assist Interv, 2005; 8(Pt 1): 811–18
23. Schneider CM, Dachs GW II, Hasser CJ et al: Robot-assisted laparoscopic ultrasound. In: Proceedings of the First international conference on Information processing in computer-assisted interventions. IPCAI'10. Berlin, Heidelberg: Springer-Verlag, 2010; 67–80
24. Schneider CM, Peng PD, Taylor RH et al: Robot-assisted laparoscopic ultrasonography for hepatic surgery. Surgery, 2012; 151(5): 756–62
25. Billings S, Deshmukh N, Kang HJ et al: System for robot-assisted real-time laparoscopic ultrasound elastography. In: Proceedings of the SPIE Medical Imaging, 2012; 67
26. Mansy HA, Grahe JR, Sandler RH: Elastic properties of synthetic materials for soft tissue modeling. Phys Med Biol, 2008; 53(8): 2115–30
27. Rivaz H, Boctor E, Foroughi P et al: Ultrasound elastography: a dynamic programming approach. IEEE Trans Med Imaging, 2008; 27(10): 1373–77
28. Rivaz H, Boctor EM, Choti MA, Hager GD: Real-time regularized ultrasound elastography. IEEE Trans Med Imaging, 2011; 30(4): 928–45
29. Su L, Link RE, Bhayani SB et al: Nerve-sparing laparoscopic radical prostatectomy: replicating the open surgical technique. Urology, 2004; 64(1): 123–27
30. McNeal JE, Redwine EA, Freiha FS, Stamey TA: Zonal distribution of prostatic adenocarcinoma. Correlation with histologic pattern and direction of spread. Am J Surg Pathol, 1988; 12(12): 897–906
31. Cohen RJ, Shannon BA, Phillips M et al: Central zone carcinoma of the prostate gland: a distinct tumor type with poor prognostic features. J Urol, 2008; 179(5): 1762–67; discussion 1767

Ultrasound Elastography Mosaicing

****

****

Abstract. Panoramic ultrasound imaging is emerging as a prevalent technique in clinical practice with a high clinical value. In the literature of ultrasound mosaicing, registering the underlying displacement field for elastography has not yet been addressed. The clinical advantages of ultrasound mosaics can be improved with the additional corresponding strain information. In this paper, we propose a technique for generating a reliable, wide field-of-view displacement field, robust to sources of decorrelation. Elastography mosaics are generated from two pairs of ultrasound images, and then from multiple image pairs. Experimental phantom data is used for the validation of the multi-image elastography mosaic. Finally, the method is extended to multiple 3D volume pairs.

1 Introduction

Compared to other imaging modalities like CT and MR, ultrasound suffers from a limited field of view. Monitoring a structure can be particularly challenging when it is too large to be visualized in a single image or 3D sweep. Size and distance measurements are unreliable in large organs. Panoramic imaging is emerging as a prevalent technique used in widening the field of view (FOV) of medical ultrasound images. Also referred to as stitching or panorama, the ultrasound mosaic aims to achieve several clinical advantages which come along with extended FOV: 1) improving the understanding of spatial relationships among structures when the size of a single image/volume is not large enough to cover the entire area, 2) allowing for measurements of size and distance in large organs and lesions, 3) allowing multi-modal registration and fusion with pre-operative data for guidance in minimally-invasive interventions.

Ultrasound elastography is a technique first proposed two decades ago by [1] for the clinical imaging of tissue stiffness. Numerous clinical applications have been investigated, among them cancer imaging [1], ablation monitoring [2], and the detection and grading of deep vein thrombosis [3]. In this work we focus on extended FOV displacement estimation for quasi-static ultrasound elastography. The tissue is imaged while it is slowly deformed using an external mechanical force and the images are used for the estimation of tissue motion or displacement [1]. Elastography maps the mechanical properties of tissue which can add valuable features to the B-mode panorama. Many clinical applications deal with large cancerous lesions which expand beyond the span of 1(one) ultrasound image [4]. An ultrasound elastography mosaic can improve the understanding of the size of

the lesion and its layout among surrounding structures. In the ablation of hepatic cancerous tissue, the size of the HIFU-induced ablative lesions often exceeds 4 cm in diameter, which is the width of a typical ultrasound transducer. Thermal lesions are not visible in conventional B-mode ultrasound but a panoramic ultrasound elastogram can help visualize the entire extent of the ablation [2], monitoring and insuring all cancerous tissue is ablated. In the assessment of venous thrombi, a combination of ultrasound B-mode and Doppler imaging help detect the presence of the blood clot, but it is elastography which can provide its age and clinical grading [3]. An in-plane ultrasound elastography mosaic can provide mapping of the thrombi all along the femoral vein. It could take up to eight mosaiced volumes to depict an entire organ like the liver or kidney [5], but having the corresponding elastography mosaic would allow for registration with pre-operative imaging data (CT or MRI) which would help with intra-operative navigation. Although the basics of medical elastography have long been defined, new clinical applications are constantly emerging are we are seeing an increasing commercial and clinical interest.

Multiple approaches have been published in the literature on 2D and 3D wide FOV ultrasound mosaics [6, 5, 7, 8], but very little of it concerns registering the underlying strain field. As various sources of decorrelation are usually affecting the computation of strain images, this problem becomes even more important when attempting to generate a unified, wide displacement field. Further more, most elastography algorithms result in qualitative strain; 2 image pairs with even very slightly different degrees of compression will produce 2 strain images in which different structures could be visible. Another problem rises in the ambiguity of the interpretation of strain images: low strain can be indicative of high stiffness but this interpretation may not be the right one if the stress field is not uniform throughout the tissue [1, 9]. To address these issues and to improve the quality of strain images, several metrics of stability, consistency/persistency and reliability have been developed [10–12]. In these paper we propose using similar techniques to select a stable pair of RF-lines which will become the *seed* for generating a reliable, wide FOV displacement field. Displacement on the *seed* line is calculated using dynamic programming and later propagated in both lateral directions of the mosaic using an analytic minimization approach [13]. Each new image pair adds to the unified displacement field. Experimental phantom data is used for the validation of the multi-image elastography mosaic. Finally, the method is extended to 3D ultrasound elastography mosaicing using multiple 3D volume pairs.

2 Methodology

Consider a sequence of radio frequency (RF) data (Im_{11}, Im_{12}) collected at position t_0, before and after the compression of tissue using a 2D ultrasound transducer (Fig. 1b). Each sequence is contains n RF-lines of length m. A second sequence (Im_{21}, Im_{22}) is collected (Fig. 1c) after the transducer has been moved in the lateral direction of the probe to position t_1, with the help of a moving stage

(Fig. 1a). A vertical stage was used to achieve an almost identical compression rate between the two sequences. The translation between the 2 image sequences is:

$$T_{lines} = T_{mm} * n/w \tag{1}$$

where w is the width of the ultrasound transducer in millimeters (mm), n is the number of RF-lines, T_{mm} is the ground truth translation in mm as read on the stage and T_{lines} is the corresponding translation as number of RF-lines. The overlap area consists of (n - T_{lines}) RF-lines (Fig. 1d).

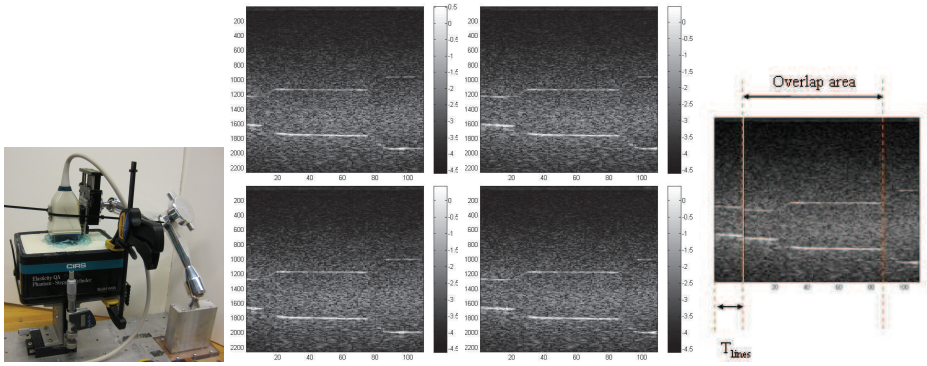

Fig. 1. Experimental setup (a). Bmode ultrasound data before and after compression for (b) position t_0, and (c) position t_1. Translation T_{lines} and the length of the overlap area are shown in (d).

Pairwise Mosaicing In Analytic Minimization (AM) elastography [13], 2D integer displacements are first obtained using dynamic programming (DP) on a single pair of RF-lines and are later propagated to produce 2D subsample displacements for the entire image. We aim to find a robust and stable *seed* RF-line in the overlap area, which also gives consistent DP integer displacement results in the two sequences. This RF-line will serve as initial guess in the AM propagation. The selection of the most stable, optimal *seed* RF-line is implemented as follows:

1. $k = 10$ $(i_1, i_2, ..., i_{10})$ random corresponding positions (RF-line pairs) are selected from the overlap area (Fig. 2-1).
2. Compute integer axial displacement for each RF-line pair: $(a_1^1, a_2^1, ..., a_{10}^1)$ and $(a_1^2, a_2^2, ..., a_{10}^2)$ (Fig. 2-2). Note: in this step, both axial and later integer displacements are computed, but from here on only axial displacement values will be used.
3. A stability test identifies and removes RF-lines which exhibit a high degree of decorrelation. The test is considered positive when the three or more positions exhibit a continuous change in the slope of displacement (Fig. 2-3) [12].

4. For the remaining positions,

$$d_k = abs(a_k^1 - a_k^2); avg_k = mean(d_k); std_k = stdev(d_k) \tag{2}$$

We select the *seed* RF-line s as the position with the minimum std_k and $avg_k < 1$ (Fig. 2-4).

5. Subinteger displacement values are calculated for RF-line s in one of the image pairs. In the Analytic Minimization (AM) method [13] we aim to calculate Δa_i and Δl_i such that the duple $(a_i + \Delta a_i, l_i + \Delta l_i)$ gives the axial and lateral displacements at the sample i. For I_1 and I_2 two ultrasound images acquired before and after deformation, the regularized cost function at the ith sample of the jth RF-line follows (Fig. 2-5):

$$\begin{aligned} &C_j(\Delta a_1, ..., \Delta a_m, \Delta l_1, ..., \Delta l_m) = \\ &= \textstyle\sum_m^{i=1} \{[I_1(i,j) - I_2(i + a_i + \Delta a_i, j + l_i + \Delta l_i)]^2 + \\ &+ \alpha \left(a_i + \Delta a_i - a_{i-1} - \Delta a_{i-1}\right)^2 + \\ &+ \beta_a \left(l_i + \Delta l_i - l_{i-1} - \Delta l_{i-1}\right)^2 + \beta_l^{'} \left(l_i + \Delta l_i - l_{i,j-1}\right)^2 \end{aligned} \tag{3}$$

where the index j was dropped for the j^{th} RF-line and $l_{i,j-1}$ is the lateral displacement of the previous RF-line (except for the *seed* line where $l_{i,j-1} = l_i$. α, β_a and $\beta_l^{'}$ are regularization terms which ensure continuity in displacements with respect to the top (axial α), and the top and left/right (lateral β_a and $\beta_l^{'}$).

6. The subinteger displacement values are propagated using AM:
   - in one sequence towards the first RF-line, and
   - in the second sequence towards the last RF-line.

   The unified displacement field will have $n + T_{lines}$ RF-lines and the stitch will be around RF-line number $s + T_{lines}$ (Fig. 2-6).
7. Generate the ultrasound elastography mosaic from the unified displacement field (Fig. 2-7).

Multi-image Mosaicing Given an existing n_t wide displacement map, computed for image pairs 1 through t, we expand our displacement map to include information from image pair $t + 1$ as follows:

1. Compute the translation T_{lines}^{t+1} between position t and position $t+1$ and the overlap area.
2. Follow steps 1 - 4 from above to select the *seed* RF-line s_{t+1}.
3. Use the subinteger values form the wide FOV displacement map at RF-line number $s_{t+1} + T_{lines}$ as *seed* values to propagate using AM:
   - in the new sequence towards the first RF-line.

   Stitch the newly computed $(s_{t+1} + T_{lines})$ lines at the beginning of the previous displacement map. The new mosaiced displacement field will have $n_t + T_{lines}^{t+1}$ RF-lines.
4. Generate the new ultrasound elastography mosaic from the updated displacement field.

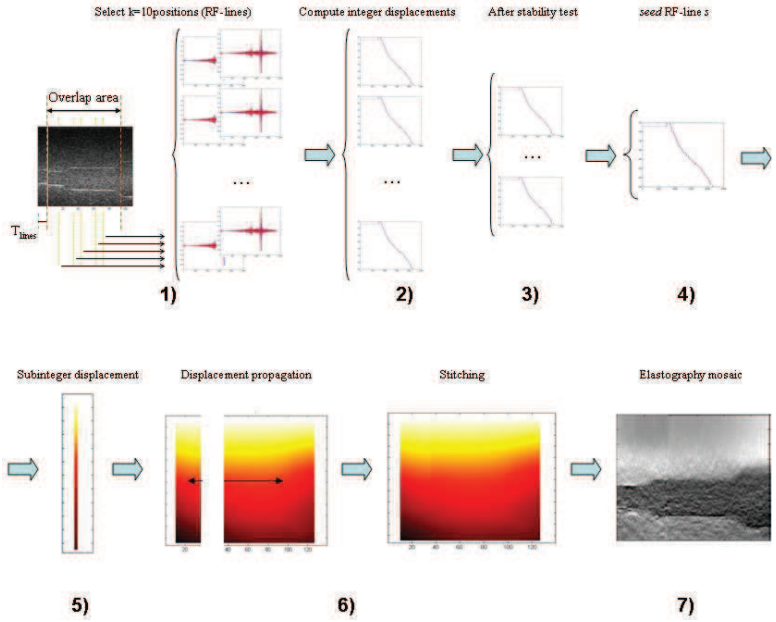

Fig. 2. Pairwise Mosaicing workflow: $k = 10$ random RF positions are selected (1), integer displacement is calculated for each position (2), some positions are identified and removed after stability test (3), the *seed* RF-line s is selected (4), subinteger displacement values are calculated for s (5), propagated in the 2 sequences and stitched (6). The ultrasound elastography mosaic is generated from the displacement field (7).

3 Results and Validation

For experimental validation we palpated a CIRS (Norfolk, VA) elastography *049a* elastography phantom (Fig. 1c) using a high-frequency ultrasound transducer (L14-5W/60) at center frequency of 10 MHz. Ultrasound RF data was acquired from an Ultrasonix system (Vancouver, BC) at 40MHz sampling rate. The *049a* phantom consists of a series of stepped cylinders of varying diameters. The transducer was placed on top of one of the cylinders, parallel with its direction. The phantom was placed on a stage which controlled the compression in the axial direction and the translation in the lateral direction (Fig. 1c). RF data sequences were acquired from 4(four) axial compression levels ($c_0 = 0$, $c_1 = 2.54$mm, $c_2 = 5.08$mm, $c_3 =$ back to 0), for each of 4(four) lateral translation positions of the transducer ($t_0 = 0$, $t_1 = 5.08$mm, $t_2 = 10.16$mm, $t_3 = 20.32$mm), for a total of 16(sixteen) data sets. The width of the ultrasound transducer L14-5W is 59mm, and as a consequence any 2 sets separated by a lateral translation had some amount of overlap.

Ultrasound elastography images were obtained for each translation position t_0 - t_3 ((Fig. 3a-d). A pairwise elastography mosaic was produced from positions t_0 and t_1 ((Fig. 3e), and then multi-image elastography mosaics from positions t_0, t_1 and t_2 ((Fig. 3f), and t_0, t_1, t_2 and t_3 ((Fig. 3g).

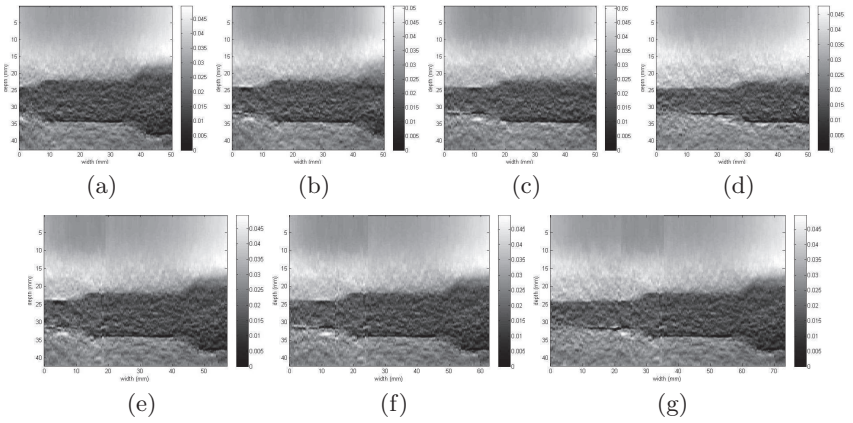

Fig. 3. Ultrasound elastography at position t_0 (a), t_1 (b), t_2 (c), t_3 (d) and elastography mosaic of positions t_0 and t_1 (e), t_0, t_1 and t_2 (f), and t_0, t_1, t_2 and t_3 (g).

Mosaicing multiple images in a pairwise fashion can cause errors to accumulate with each new added image. To calculate this error we computed the wide FOV displacement map from positions t_0 and t_3, and compared it with the multi-image displacement map from positions t_0, t_1, t_2 and t_3 added consecutively. The random search algorithm was run 5 times and the results averaged. For the resulting displacement maps, we computed an absolute difference per pixel, as well as mean and standard deviation absolute difference for the entire FOV.

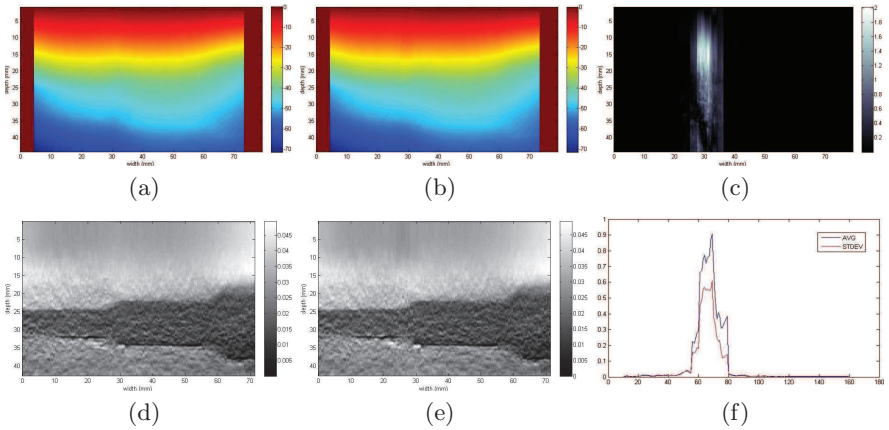

Fig. 4. Panoramic displacement map of positions t_0 and t_3 (a), and of positions t_0, t_1, t_2 and t_3 (b), the absolute difference between them (c), and the mean and standard deviation of this difference, per line (d). The unit of displacement is pixels. Corresponding ultrasound elastography mosaics of positions t_0 and t_3 (e), and t_0, t_1, t_2 and t_3 (f).

Figure 4 shows the results of the validation experiment. The two panoramic displacement maps agree almost exactly; the absolute difference for the entire

image had a mean of 0.0755 and a standard deviation of 0.2386 pixels. The maximum difference was 2.0168 pixels and it did not exceed 1 pixel on a mean, per-line basis. For a metric correspondent, 2.0168 pixels, is the equivalent of 0.0406 mm in the axial direction. Once the displacement maps are converted in elastogram mosaics (Fig. 4 e,f), the difference becomes indistinguishable even on close inspection. With the clinical application in mind, we conclude that these small differences are acceptable.

4 3D mosaicing

For 3D validation, RF data was acquired using an Ultrasonix system (Vancouver, BC) at 20MHz sampling rate. The CIRS phantom was palpated with a 38mm width linear 4D volumetric transducer (4DL14-5/38). As with the 2D experiment, the phantom was placed on a stage to controll the compression in the axial direction and the translation in the lateral direction (Fig. 1c). RF data sequences were acquired from 4(four) axial compression levels ($c_0 = 0$, $c_1 = 2.54$mm, $c_2 = 5.08$mm, $c_3 =$ back to 0), for each of 5(five) lateral translation positions of the transducer ($t_0 = 0$, $t_1 = 5.08$mm, $t_2 = 10.16$mm, $t_3 = 20.32$mm, $t_4 = 22.86$mm), for a total of 20(twenty) data sets. Figure 5 shows the results.

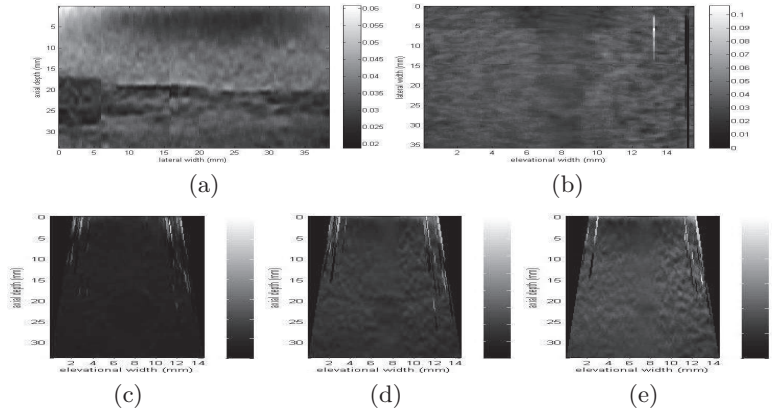

(a) (b) (c) (d) (e)

Fig. 5. 3D ultrasound elastography mosaic: axial-lateral plane (a), lateral-elevational plane (b), and 3 axial-elevational planes through 3 different diameters of the stepped cylinder (d)

5 Discussion and Conclusion

We have presented an algorithm for generating reliable multi-image ultrasound elastography mosaics, robust to regions of decorrelation. Panoramic B-mode ultrasound has been reported with success in the literature and, with the addition of corresponding elastograms, an ultrasound system with these capabilities has

great potential in clinical diagnostic and monitoring. Elastography has the advantage that is requires no additional hardware to be implemented, and a majority of commercial ultrasound systems now present an elastography interface. Furthermore, efforts are under way to incorporate electromagnetical (EM) tracking in ultrasound transducers. The work presented here makes a case for in-plane mosaicing where translation is the only component of the transformation. One can easily envision an ultrasound system equipped with a tracked transducer, where RF frames can be tracked and, based on their position, suitable frames can be selected for elastography [14], as well as for elastography mosaics.

References

1. Ophir, J., Alam, S.K., Garra, B., Kallel, F., Konofagou, E., Krouskop, T., Varghese, T.: Elastography: ultrasonic estimation and imaging of the elastic properties of tissues. Proceedings of the Institution of Mechanical Engineers. Part H, Journal of Engineering in Medicine **213**(3) (1999) 203–233
2. Varghese, T., Zagzebski, J., Lee Jr., F.: Elastographic imaging of thermal lesions in the liver in vivo following radiofrequency ablation: preliminary results. Ultrasound in Medicine & Biology **28**(1112) (December 2002) 1467–1473
3. Emelianov, S., Chen, X., ODonnell, M., Knipp, B., Myers, D., Wakefield, T., Rubin, J.: Triplex ultrasound: elasticity imaging to age deep venous thrombosis. Ultrasound in Medicine & Biology **28**(6) (June 2002) 757–767
4. Garra, B., Cespedes, E., Ophir, J., Spratt, S., Zuurbier, R., Magnant, C., Pennanen, M.: Elastography of breast lesions: initial clinical results. Radiology **202**(1) (1997) 79–86
5. Poon, T.C., Rohling, R.N.: Three-dimensional extended field-of-view ultrasound. Ultrasound in Medicine & Biology **32**(3) (March 2006) 357–369
6. Gee, A.H., Treece, G.M., Prager, R.W., Cash, C.J., Berman, L.: Rapid registration for wide field of view freehand three-dimensional ultrasound. IEEE Transactions on Medical Imaging **22**(11) (November 2003) 1344–1357
7. Wachinger, C., Wein, W., Navab, N.: Registration strategies and similarity measures for three-dimensional ultrasound mosaicing. Academic Radiology **15**(11) (November 2008) 1404–1415
8. Rajpoot, K., Noble, J.A., Grau, V., Szmigielski, C., Becher, H.: Multiview RT3D echocardiography image fusion. In Ayache, N., Delingette, H., Sermesant, M., eds.: Functional Imaging and Modeling of the Heart. Volume 5528. Springer Berlin Heidelberg, Berlin, Heidelberg (2009) 134–143
9. Lindop, J.E., Treece, G.M., Gee, A.H., Prager, R.W.: 3d elastography using freehand ultrasound. Ultrasound in Medicine & Biology **32**(4) (2006) 529 – 545
10. Jiang, J., Hall, T.J., Sommer, A.M.: A novel image formation method for ultrasonic strain imaging. Ultrasound in Medicine & Biology **33**(4) (2007) 643 – 652
11. Lindop, J., Treece, G., Gee, A., Prager, R.: An intelligent interface for freehand strain imaging. Ultrasound in Medicine & Biology **34**(7) (2008) 1117 – 1128
12. Fleming, I., Rivaz, H., Boctor, E., Hager, G.: Robust dynamic programming method for ultrasound elastography. SPIE **8320**(1) (2012) 83201–83206
13. Rivaz, H., Boctor, E., Choti, M., Hager, G.: Real-time regularized ultrasound elastography. IEEE Transactions on Medical Imaging **30**(4) (April 2011) 928–945
14. Foroughi, P., Rivaz, H., Fleming, I.N., Hager, G.D., Boctor, E.M.: Tracked ultrasound elastography (true). In: Proceedings of. MICCAI'10 (2010) 9–16